Properties of Graphene in an External Magnetic Field

- Bachelorarbeit -

der Philosophisch-naturwissenschaftlichen Fakultät
der Universität Bern
vorgelegt von

Sacha Schwarz

2011

Betreut durch

Prof. Dr. U.-J. Wiese

Albert Einstein Center for Fundamental Physics
Institut für theoretische Physik, Universität Bern

Abstract

In my bachelor thesis, I present an introduction to the new material graphene, a mono molecular layer of graphite with hexagonal structure. Based on the microscopic Hubbard model as well as on the Dirac equation in a effective low-energy theory, I describe the motion of massless, relativistic, quasi-free Dirac fermions on the graphene lattice. First, I develop in both cases a Hamiltonian which I diagonalize in a second step for extracting the dispersion relation. Furthermore, I extend both Hamiltonians in the case of an external magnetic field to describe graphene's behavior in a magnetic flux.

Contents

Chapter 1

Introduction

The aim of this bachelor thesis is to give an introduction to the electronic properties of graphene as well as to graphene's behavior in an external magnetic field perpendicular to it. After a brief motivation in the following section 1.1, we will work out the basic properties of graphene in chapter 2 and focus on the geometry of the 2D honeycomb lattice. In chapter 3, we first develop a Hamiltonian based on the single-band Hubbard model for describing the electron motion on the graphene lattice in a microscopic manner. Furthermore in chapter 4, we describe the electron motion on the graphene lattice, this time at low energy by developing the Hamiltonian in the framework of an effective theory. Moreover, in this chapter we explain why the interacting electrons in graphene are characterized by massless, relativistic Dirac fermions and present first evidence thereof. Finally, in chapter 5, we extend the developed Hamiltonians to incorporate an external magnetic field. First, we consider the microscopic model of chapter 3 with an additional magnetic field. In a second step, we introduce the magnetic field in the effective theory of chapter 4, as well, and interpret the consequences. It turns out, that a magnetic field applied to graphene gives rise to discrete Landau levels which are essentially important in the explanation of a anomalous quantum Hall effect in graphene.

1.1 General Facts and Historical Aspects

A very important element for life is the carbon atom C [1]. It is one of the most abundant elements in the universe as well as in the Earth's crust. It is also found in all known life forms. Therefore, it is not astonishing that carbon is called the chemical basis of life. By considering carbon-based systems we find several structures which bond their carbon atoms in different manners, we call them allotropes. The relatively well-known allotropes of carbon are diamond and graphite. Both are made of carbon atoms but have different properties. Diamond is an extremely hard dielectric material and crystallizes in a cubic system. It consists of four sp^3 hybridised orbitals, i.e. all outer four valence electrons of the carbon atom permit covalent bondings to four other carbon atoms. In other words, they are all localised between the atoms in covalent bonding and form a tetrahedral geometry. However, graphite is one of the softest material and crystallizes in a hexagonal system. It consists of three sp^2 hybridised orbitals and is an electric conductor. As we can see, both allotropes have nearly opposite properties. Let us consider graphite in more detail. It is made of several weakly bonded planar layers where the carbon atoms are arranged in a hexagonal structure. This is the result of the sp^2 hybridised orbitals. Every carbon atom of this allotrope uses only three of its four

outer electrons in covalent bonding to three other carbon atoms. Therefore, they arrange themselves in a plane and form a strongly bonded, planar lattice with hexagonal structure. Unlike diamond, we see that each carbon atom in graphite has one delocalized electron. It is free to move through the entire plane. For this reason, graphite conducts electricity only along the planes of carbon atoms.
We understand the link between graphite and graphene by looking at history. In 1859, the chemist Benjamin C. Brodie prepared graphite oxide by treating graphite with strong oxidizers so that the distance between several layers became much larger and irregular. In basic solutions, the graphite oxide finally disperses and yields mono-molecular sheets, known as graphene oxide. At that time, Brodie was already thinking about a tear-resistant graphite oxide paper [2]. In 1962, Hanns-Peter Boehm published his study on few-layer graphene and formed the expression *graphene*, a mono-molecular layer of carbon atoms arranged in a planar hexagonal lattice [3]. During the 20th century, hundreds of researchers have entered this area until 2004. In that year, Andre Geim and Konstantin Novoselov realised the first method to produce mono-molecular graphene layers by graphite oxide reduction. By referring to Boehm's forming of the expression, Geim describes graphene with the following words:

> *"graphene is stronger and stiffer than diamond, yet can be stretched by a quarter of its length, like rubber. Its surface area is the largest known for its weight."* - Andre Geim

In 2010, Geim and Novoselov were awarded the Nobel Prize in Physics for *Groundbreaking Experiments Regarding the Two-Dimensional Material graphene* [4].
After this historical introduction, it is important to mention the difference between the graphene lattice and other crystal lattices. In quantum field theory and statistical mechanics, the Mermin-Wagner theorem states that a 2D lattice can not stay stable at finite temperature [5]. Fluctuations persuade the crystal lattice to roll up or to agglutinate. In the case of graphene, these fluctuations are suppressed by anharmonic couplings between bending and stretching modes in the lattice. It is argued that graphene is not flat but a ripped 2D lattice [6].
We can see in Fig. 1.1, graphene can be understood as a 2D building material for carbon materials of all other dimensions. With a 2D lattice like graphene, it is possible to build up materials of 0D, 1D and 3D.

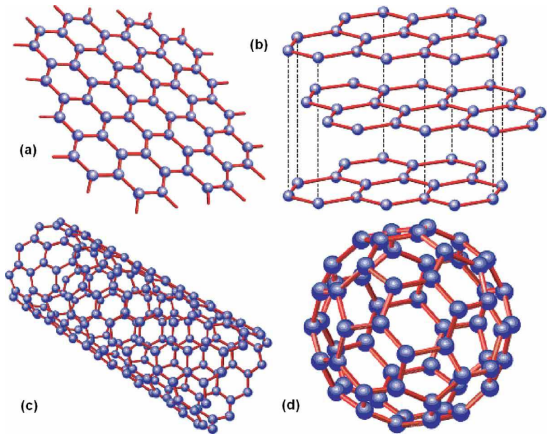

Figure 1.1: graphene (Fig.a) can be stacked into 3D graphite (Fig.b), rolled into 1D nanotubes (Fig.c) or wrapped up into 0D Fullerenes (Fig.d). [7]

In summary, graphene is harder than diamond but flexible like a piece of iron sheet and a much better conductor of electricity than other materials. With such properties, graphene could revolutionize the whole micro- and computer-technology (see chapter 6).

Chapter 2

Properties of the Honeycomb Lattice

In this chapter we start by discussing general properties of the graphene lattice which are used in further chapters. On this account, we consider an infinite 2D graphene lattice, i.e. a lattice which is made up of carbon atoms arranged in a hexagonal manner like a honeycomb (see Fig. 2.1). We neglect here the aspect of ripping and consider a flat honeycomb lattice. As commonly done in solid state physics (see e.g. [8]), we identify the unit cell as well as the primitive vectors of the honeycomb lattice. In a second step, we construct the first Brillouin zone with the according primitive vectors of the reciprocal lattice and briefly discuss some symmetries of the honeycomb lattice. Finally, we calculate the normalizing constant for the hexagonal lattice in the Fourier transform which links the position space with the momentum space, i.e. the discrete lattice with the k-space as continuum. Using the constructed Fourier transform, we are able to diagonalize the Hamiltonian in chapter 3.

2.1 A bipartite non-Bravais lattice

A crystal lattice is called a Bravais lattice when *it is an infinite array of discrete points with an arrangement and orientation that appears exactly the same, from whichever of the points the array is viewed* [9]. With this definition, it is easily understood that a hexagonal lattice is non-Bravais, because only next-to-nearest neighbor points appear with the same arrangement and orientation. Therefore, in graphene we are dealing with two triangular Bravais sub-lattices A and B which together form the non-Bravais graphene lattice. The difference between the sub-lattices A and B is a rotation of π. Expressing this in a more formal way, we choose the two primitive lattice vectors in the following way:

$$\vec{a}_1 = a \begin{pmatrix} 1 \\ 0 \end{pmatrix}, \quad \vec{a}_2 = a \begin{pmatrix} \frac{1}{2} \\ \frac{\sqrt{3}}{2} \end{pmatrix}, \tag{2.1}$$

where a denotes the distance between two lattice points, which has an experimentally determined length of about 2.46Å[7]. The origin of these primitive vectors is set in the middle of an optional honeycomb, so that a linear combination of $\vec{a}_1$ and $\vec{a}_2$ with integer prefactors characterizes a space point $\vec{x}$, i.e. we have a set of vectors defined by

$$X := \{\vec{x} \in \mathbb{R}^2 | \vec{x} = n_1\vec{a}_1 + n_2\vec{a}_2,\, n_1, n_2 \in \mathbb{Z}\}. \tag{2.2}$$

In order to work with these primitive vectors in further chapters, we are interested in the positions of carbon atoms and not in the centers of hexagons. With the two unit-vectors $\vec{e}_A$ and $\vec{e}_B$, given by

$$\vec{e}_A = a \begin{pmatrix} \frac{1}{2} \\ \frac{\sqrt{3}}{6} \end{pmatrix}, \quad \vec{e}_B = -a \begin{pmatrix} \frac{1}{2} \\ \frac{\sqrt{3}}{6} \end{pmatrix}, \tag{2.3}$$

we can distinguish between the two sub-lattices and also characterize the whole lattice by a space vector, i.e. with the set of vectors of each Bravais sub-lattices

$$X_A := X + \vec{e}_A = \{\vec{x} \in \mathbb{R}^2 | \vec{x} = n_1\vec{a}_1 + n_2\vec{a}_2 + \vec{e}_A,\, n_1, n_2 \in \mathbb{Z}\}, \tag{2.4}$$

$$X_B := X + \vec{e}_B = \{\vec{x} \in \mathbb{R}^2 | \vec{x} = n_1\vec{a}_1 + n_2\vec{a}_2 + \vec{e}_B,\, n_1, n_2 \in \mathbb{Z}\}, \tag{2.5}$$

we can describe the entire non-Bravais graphene lattice

$$X_G := X_A \oplus X_B. \tag{2.6}$$

The property of the graphene lattice in Eq. (2.6) belongs to the class of bipartite lattices. Therefore, graphene is a bipartite non-Bravais lattice with two carbon atoms per unit cell, illustrated in Fig. 2.1.

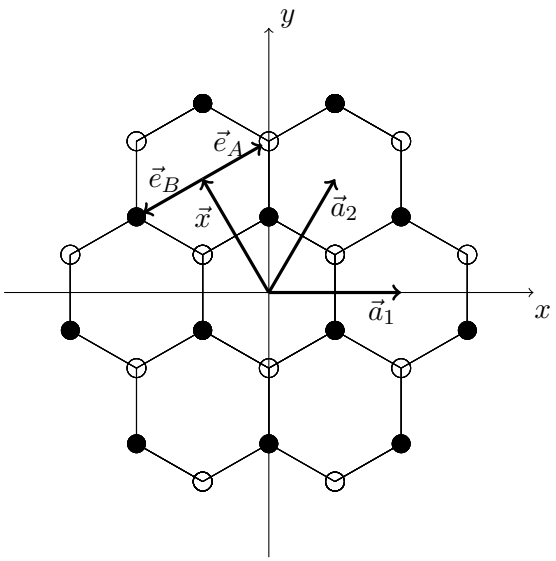

Figure 2.1: The primitive vectors $\vec{a}_1$ and $\vec{a}_2$, the space vector $\vec{x}$ connecting the centers of two hexagons, as well as the unit-vectors $\vec{e}_A$ and $\vec{e}_B$ distinguishing the sub-lattice A (○) and B (●).

For completeness we briefly discuss some symmetries of the graphene lattice. An important symmetry is the shift symmetry on each sub-lattice. This symmetry was introduced by the two primitive vectors $\vec{a}_1$ and $\vec{a}_2$ in Eq. (2.1) and maps $A \to A$ and $B \to B$. Obviously, the shift transformation $A \to B$ is not defined according to the primitive vectors.
Another important symmetry which should be mentioned here is the rotation symmetry R. We can see that a rotation by $\frac{\pi}{6}$ with the centre of rotation in the center of a hexagon maps the sub-lattice A onto B and vice versa, i.e. $A \to B$ and $B \to A$.

2.2 The reciprocal lattice

For the two sub-lattices A and B, defined in Eq. (2.4) and Eq. (2.5), the primitive vectors in Eq. (2.1) are the same. The only difference between them is found in the two different unit-vectors $\vec{e}_A$ and $\vec{e}_B$, i.e.

$$\vec{e}_A = -\vec{e}_B. \tag{2.7}$$

In momentum space, the primitive reciprocal vectors $\vec{b}_1$ and $\vec{b}_2$ are the same for both sub-lattices A and B. With Eq. (2.1) and the Laue condition

$$\vec{a}_i \cdot \vec{b}_j = 2\pi\delta_{ij}, \quad i,j \in 1,2, \tag{2.8}$$

we obtain the primitive vectors of the reciprocal lattice, which are given by

$$\vec{b}_1 = \frac{4\pi}{\sqrt{3}\,a}\begin{pmatrix} \frac{\sqrt{3}}{2} \\ -\frac{1}{2} \end{pmatrix}, \quad \vec{b}_2 = \frac{4\pi}{\sqrt{3}\,a}\begin{pmatrix} 0 \\ 1 \end{pmatrix}. \tag{2.9}$$

The corresponding first Brillouin zone is illustrated together with the obtained primitive vectors in Fig. 2.2. We see that the first Brillouin zone forms a hexagon, which is rotated by $\frac{\pi}{12}$ compared to the hexagonal structure in position space.

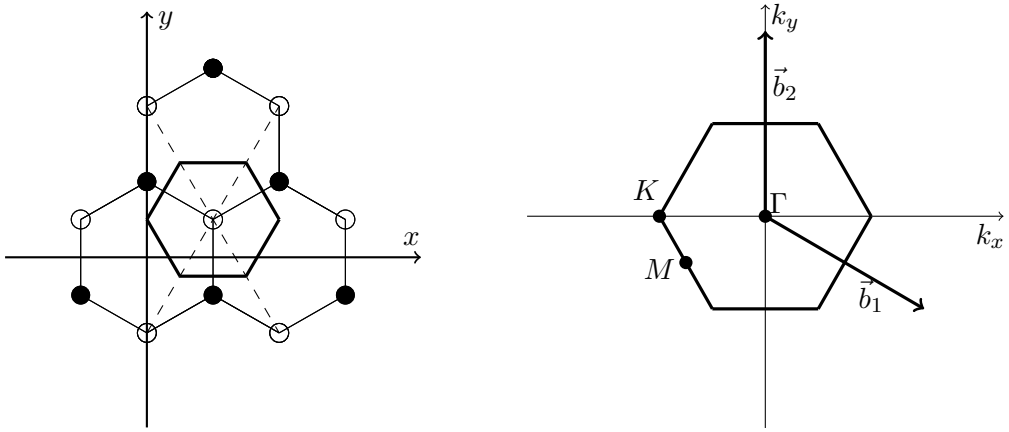

Figure 2.2: The corners of the first Brillouin zone are constructed by determining the mean distance between nearest-neighbor points of the same sub-lattice. On the left, there is the first Brillouin zone, constructed for sub-lattice A. On the right, the calculated primitive vectors $\vec{b}_1$ and $\vec{b}_2$ are illustrated together with the first Brillouin-zone as well as the points M, Γ and K, which come up important in the following chapter 3.

Fig. 2.2 shows only the first Brillouin zone for sub-lattice A. If we also construct it for sub-lattice B, several corners of sub-lattice A are at the same place as corners of sub-lattice B. This implies that the resulting Brillouin zone of the graphene lattice is a combination of both sub-lattices. Note that we find at every lattice point at most two fermions with the opposite spin.
A more general but important remark is related to the periodicity of the Brillouin zone. All momenta can be shifted into the first Brillouin zone, because A and B are Bravais lattices. This implies that only the momenta in the first Brillouin zone are important for further

calculations.
To complete this section, let us just highlight the corners of the first Brillouin zone. They are discussed in more detail in chapter 3 and chapter 4. In the first Brillouin zone, we count six corners, which we arrange in two sets, i.e. they are given by

$$K = \left\{ \frac{4\pi}{\sqrt{3}\,a} \begin{pmatrix} \frac{1}{\sqrt{3}} \\ 0 \end{pmatrix}, \frac{4\pi}{\sqrt{3}\,a} \begin{pmatrix} -\frac{\sqrt{3}}{6} \\ \frac{1}{2} \end{pmatrix}, \frac{4\pi}{\sqrt{3}\,a} \begin{pmatrix} -\frac{\sqrt{3}}{6} \\ -\frac{1}{2} \end{pmatrix} \right\}, \tag{2.10}$$

$$K' = \left\{ \frac{4\pi}{\sqrt{3}\,a} \begin{pmatrix} -\frac{1}{\sqrt{3}} \\ 0 \end{pmatrix}, \frac{4\pi}{\sqrt{3}\,a} \begin{pmatrix} \frac{\sqrt{3}}{6} \\ -\frac{1}{2} \end{pmatrix}, \frac{4\pi}{\sqrt{3}\,a} \begin{pmatrix} \frac{\sqrt{3}}{6} \\ \frac{1}{2} \end{pmatrix} \right\}. \tag{2.11}$$

Referring to the periodicity of the Brillouin zone, only two corners are actually important, because the others can be obtained by some shift operations and are identified with the first corner by periodic boundary conditions. For this reason, we choose a representative of the set K in Eq. (2.10) and K' in Eq. (2.11). We redefine K and K' and use only the corners

$$K = \frac{4\pi}{\sqrt{3}\,a} \begin{pmatrix} \frac{1}{\sqrt{3}} \\ 0 \end{pmatrix}, \quad K' = \frac{4\pi}{\sqrt{3}\,a} \begin{pmatrix} \frac{\sqrt{3}}{6} \\ \frac{1}{2} \end{pmatrix}, \tag{2.12}$$

for further calculations. These two points K and K' are of particular importance for the physics of graphene and are named Dirac points for reasons that will become clear later.

2.3 Fourier transform

The link between position space and momentum space is given by the Fourier transform. The position space contains discrete points whereas the momentum space is continuous. In order to be able to transform operators from one space to the other, we have to construct the appropriate Fourier transform.
First, we define the Fourier transform of a complex function $f_{\vec{x}} : X_G \to \mathbb{C}$ with discrete values $\vec{x} \in X_G$. Using the discrete position vectors $\vec{x}$, we obtain the discrete Fourier transform

$$\tilde{f}(\vec{k}) := \sum_{\vec{x} \in X_G} f_{\vec{x}} \exp(-i\vec{k} \cdot \vec{x}), \tag{2.13}$$

for all $\vec{k} \in \mathbb{R}^2$. According to the Laue condition in Eq. (2.8), the scalar product of space vector $\vec{x} \in X_G$ and momentum vector $\vec{k} \in \mathbb{R}^2$ yields

$$\exp(i\,\vec{k} \cdot \vec{x}) = 1 \Longleftrightarrow \vec{k} \cdot \vec{x} = 2\pi n,\ n \in \mathbb{Z}, \tag{2.14}$$

and implies that the discrete Fourier transform of Eq. (2.13) does not violate the periodic property of the momentum vector $\vec{k}$. For all $\vec{x} \in X_G$ and $\vec{k}' \in \mathbb{R}^2$, we obtain

$$\tilde{f}(\vec{k} + \vec{k}') = \sum_{\vec{x} \in X} f_{\vec{x}} \exp(-i(\vec{k} + \vec{k}') \cdot \vec{x}) = \sum_{\vec{x} \in X} f_{\vec{x}} \exp(-i\vec{k} \cdot \vec{x}) \underbrace{\exp(-i\vec{k}' \cdot \vec{x})}_{=1} = \tilde{f}(\vec{k}). \tag{2.15}$$

In a second step, we consider the integral of the inverse Fourier transform $\tilde{f}(\vec{k})$. According to section 2.2, the continuous momentum space $\mathbb{R}^2$ can be decomposed into a direct sum, which is given by

$$B \oplus K = \{\vec{x} \in \mathbb{R}^2 | \vec{x} = \vec{b} + \vec{k},\, \vec{b} \in B, \vec{k} \in K\} = \mathbb{R}^2. \tag{2.16}$$

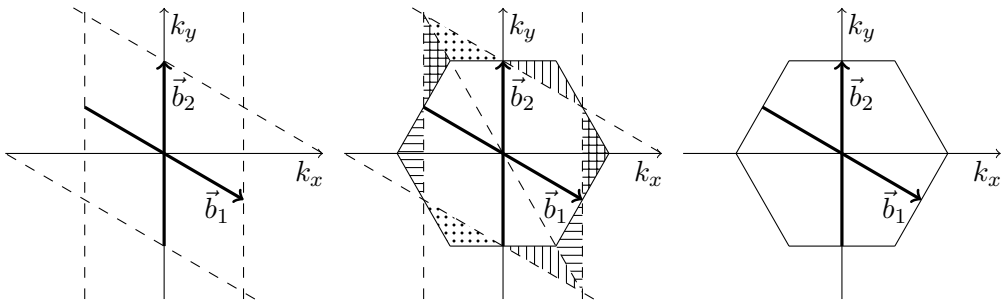

Figure 2.3: The figure in the middle illustrates the relation between the rhombic (left figure) and the hexagonal (right figure) Brillouin-zone.

A possible method to evaluate the inverse Fourier transform over a hexagon as integration area would be an evaluation over a quadrilateral.
When we are thinking about a possibility to transform a hexagon into a tetragon in order to integrate just over two simple 1-dimensional intervals, we obtain Fig 2.3 as a possibility to integrate along the primitive vectors $\vec{b}_1$ and $\vec{b}_2$. With this parametrization, the problem is simpler to solve. Given Fig. 2.3 above, we are able to use an alternative choice of the first Brillouin zone which is given by

$$B = \{\vec{k} = m_1\vec{b}_1 + m_2\vec{b}_2 \in \mathbb{R}^2 | -\frac{1}{2} \leq m_1, m_2 < \frac{1}{2}\}. \tag{2.17}$$

The corresponding inverse Fourier transform

$$f_{\vec{x}} = \int_B d^2k\, \tilde{f}(\vec{k})\, \exp(i\,\vec{k}\cdot\vec{x}) \tag{2.18}$$

to Eq. (2.13) yields, together with the boundary values of Eq. (2.17)

$$\begin{aligned} f_{\vec{x}} =& \int_{-\frac{1}{2}}^{\frac{1}{2}} dm_1 \int_{-\frac{1}{2}}^{\frac{1}{2}} dm_2\, \tilde{f}(m_1\vec{b}_1 + m_2\vec{b}_2) \exp(i(m_1\vec{b}_1 + m_2\vec{b}_2)\cdot\vec{x}) \\ =& \frac{\sqrt{3}\,a^2}{8\pi^2} \int_B d^2k\, \tilde{f}(\vec{k}) \exp(i\vec{k}\cdot\vec{x}), \end{aligned} \tag{2.19}$$

where we have used the substitution

$$k_x = \frac{2\pi}{a}m_1,\; k_y = \frac{4\pi}{\sqrt{3}a}\left(-\frac{1}{2}m_1 + m_2\right) \quad \Longrightarrow \quad m_1 = \frac{a}{2\pi}k_x,\; m_2 = \frac{a}{4\pi}k_x + \frac{\sqrt{3}\,a}{4\pi}k_y, \tag{2.20}$$

and the corresponding Jacoby determinant

$$det\left(\frac{\partial(m_1, m_2)}{\partial(k_x, k_y)}\right) = \left|\begin{pmatrix} \frac{a}{2\pi} & 0 \\ \frac{a}{4\pi} & \frac{\sqrt{3}a}{4\pi} \end{pmatrix}\right| = \frac{\sqrt{3}\,a^2}{8\,\pi^2}, \tag{2.21}$$

which is just the inverse of the area of the first Brillouin zone, i.e.

$$A_{BZ} = \frac{8\,\pi^2}{\sqrt{3}\,a^2}. \tag{2.22}$$

Finally, we can identify the δ-operators

$$\delta_{\vec{x},0} = \frac{\sqrt{3}\,a^2}{8\pi^2} \int_B d^2k \, \exp(i\vec{k} \cdot \vec{x}), \tag{2.23}$$

$$\delta(\vec{k}) = \frac{\sqrt{3}\,a^2}{8\pi^2} \sum_{\vec{x}} \exp(-i\vec{k} \cdot \vec{x}). \tag{2.24}$$

With these operators in Eq. (2.23) and Eq. (2.24) above, we are at last prepared for calculations in further chapters. In appendix A, we present a short proof that we are indeed allowed to use the proposed parametrization.

Chapter 3

Microscopic Model for Interacting Fermions

Every carbon atom of the graphene lattice uses three of its four electrons in covalent bounding to three other carbon atoms, while the fourth electron is free to move through the lattice by tunnelling effects. In order to be able to describe these free electrons, we use a simple microscopic model, the so-called single-band Hubbard model (c.f. [10]). We interpret the crystal lattice as a periodic potential which has a minimum at every carbon ion. The free electrons feel an attractive force exerted by this periodic potential and tunnel from ion to ion. In the Hubbard model, the tunnelling effect is described by the hopping of electrons from ion to ion. Obviously, these fermions are not free in respect to the potential, i.e. we are talking about quasi-free electrons. [8]. With the relation between Energy E and momentum $\vec{k}$, the so-called dispersion relation, we are able to identify energy bands of allowed or forbidden quasi-free electron energy states.
In this chapter 3, we primarily construct a Hamiltonian $\mathcal{H}$ based on the single band Hubbard model by introducing electron creation and annihilation operators. This Hamiltonian $\mathcal{H}$ describes hopping between nearest-neighbor lattice sites and yields the dispersion relation $E(\vec{k})$ which reveals the full band structure of graphene. In a second step, the quasi-free electrons are allowed to hop between nearest-neighbor and next-to-nearest-neighbor sites as well. As a result of this expansion, we obtain a asymmetry of the energy spectrum $E(\vec{k})$.

3.1 Electron Creation and Annihilation Operators

We start in this section with the introduction of new operators. The creation operator $c^\dagger_{s,\vec{x}}$ creates while the annihilation operator $c_{s,\vec{x}}$ annihilates an electron state at the lattice site $\vec{x}$ with spin s. Since electrons are fermions, they have only two possible spin orientations $s = \pm\frac{1}{2} = \uparrow, \downarrow$ and they are subject to the Pauli exclusion principle. To avoid electron states of the same spin s at the same lattice site $\vec{x}$, we introduce the anti-commutators of $c^\dagger_{s,\vec{x}}$ and $c_{s,\vec{x}}$ which are given by

$$\{c_{s,\vec{x}}\,,\, c^\dagger_{s',\vec{x}'}\} = \delta_{ss'}\delta_{\vec{x}\vec{x}'}, \quad \{c_{s,\vec{x}}\,,\, c_{s',\vec{x}'}\} = 0, \quad \{c^\dagger_{s,\vec{x}}\,,\, c^\dagger_{s',\vec{x}'}\} = 0, \tag{3.1}$$

where the anti-commutator of two operators A and B is defined as

$$\{A, B\} = AB + BA. \tag{3.2}$$

With Eq. (3.1), we see that the Pauli principle is obeyed by trying to create or annihilate two electrons of the same spin s at the same lattice site $\vec{x}$, i.e. we obtain in both cases

$$c^{\dagger 2}_{s,\vec{x}} = \frac{1}{2}\{c^{\dagger}_{s,\vec{x}}\,,\, c^{\dagger}_{s',\vec{x}'}\} = 0, \quad c^{2}_{s,\vec{x}} = \frac{1}{2}\{c_{s,\vec{x}}\,,\, c_{s',\vec{x}'}\} = 0. \tag{3.3}$$

Another combination of both operators is their product which yields the number operator $n_{\vec{x}}$ for electrons at the site $\vec{x}$ which is given by

$$n_{\vec{x}} = \sum_{s} c^{\dagger}_{s,\vec{x}}\, c_{s,\vec{x}}. \tag{3.4}$$

With the sum over all lattice sites $\vec{x}$, we obtain the total number N of quasi-free electrons in graphene.
Finally, we consider the electron states in general. The so-called vacuum state $|0\rangle$, i.e. the state without any electrons, is described by

$$c_{s,\vec{x}}\,|0\rangle = 0, \tag{3.5}$$

for both spin orientations s and all lattice sites $\vec{x}$. All other electron states of the honeycomb lattice are characterized by a linear combination of the states

$$|\psi\rangle = \prod_{\vec{x}} \left(c^{\dagger}_{\uparrow,\vec{x}}\right)^{n_{\uparrow,\vec{x}}} \left(c^{\dagger}_{\downarrow,\vec{x}}\right)^{n_{\downarrow,\vec{x}}} |0\rangle, \tag{3.6}$$

where the occupation number is $n_{s,\vec{x}} \in \{0,1\}$ for both spins s. Thus, each lattice site can either be vacant or occupied by a fermion with spin up $s = \uparrow$, by one with spin down $s = \downarrow$ or by two fermions with opposite spins.

3.2 Single Band Hubbard Model

We consider the honeycomb lattice with one electron at each lattice site and allow them to hop between nearest-neighbor carbon ions. The whole inner structure of every carbon atom is neglected in this process, since we concentrate only on the tunnelling effect of the quasi-free electrons. With the electron creation and annihilation operator of section 3.1, we characterize electron hopping as an electron of spin s which is first annihilated at a lattice site $\vec{x}$ and then recreated at the nearest-lattice site $\vec{y}$. To describe this quantum mechanical motion of electrons on the graphene lattice, we use the mentioned Hubbard model. The Hamiltonian based on this model is given by

$$\mathcal{H} = -t \sum_{\substack{<\vec{x},\vec{y}> \\ s=\uparrow,\downarrow}} \left(c^{\dagger}_{s,\vec{x}}\, c_{s,\vec{y}} + c^{\dagger}_{s,\vec{y}}\, c_{s,\vec{x}}\right), \tag{3.7}$$

where the hopping parameter t controls the tunnelling amplitude. It is given in units of energy and has an experimental value of about $2.8eV$ [7]. As we see in Eq. (3.7), the energy operator $\mathcal{H}$ is a sum of all electron hopping terms between nearest-neighbors, calculated over all possible lattices sites $\vec{x}$. Note that this Hamiltonian is Hermitian, i.e. $\mathcal{H} = \mathcal{H}^{\dagger}$.
To interpret the general form of the Hamiltonian in Eq. (3.7) in the special case of honeycomb lattice, we use the definitions of chapter 2. Due to the shift invariance of one single hexagon of

the graphene lattice, we only have to consider one single hexagon for the interacting quasi-free electrons. By beginning with an electron creation at the lattice site $\vec{x}+\vec{e}_B+\vec{a}_1$ and electron annihilation at the lattice site $\vec{x}+\vec{e}_A$, we go anti-clockwise and generate six different terms of electron hopping between nearest-neighbors. Therefore, the Hamiltonian for a graphene lattice is given by

$$\begin{aligned}\mathcal{H} = -t \sum_{s,\,\vec{x}} \big[& c^\dagger_{s,\,\vec{x}+\vec{e}_B+\vec{a}_1}\, c_{s,\,\vec{x}+\vec{e}_A} + c^\dagger_{s,\,\vec{x}+\vec{e}_A}\, c_{s,\,\vec{x}+\vec{e}_B+\vec{a}_2} + c^\dagger_{s,\,\vec{x}+\vec{e}_B+\vec{a}_2}\, c_{s,\,\vec{x}+\vec{e}_A-\vec{a}_1} + \\ & c^\dagger_{s,\,\vec{x}+\vec{e}_A-\vec{a}_1}\, c_{s,\,\vec{x}+\vec{e}_B} + c^\dagger_{s,\,\vec{x}+\vec{e}_B}\, c_{s,\,\vec{x}+\vec{e}_A-\vec{a}_2} + c^\dagger_{s,\,\vec{x}+\vec{e}_A-\vec{a}_2}\, c_{s,\,\vec{x}+\vec{e}_B+\vec{a}_1} \big] \end{aligned} \tag{3.8}$$

The aim of this section is the diagonalization of the Hamiltonian $\mathcal{H}$ in Eq. (3.8), in order to extract the dispersion relation $E(\vec{k})$. First, we transform the Hamiltonian from position space into momentum space, so that we can simplify it. In a second step, we diagonalize it in section 3.2.2 and finally extract in section 3.2.3 the dispersion relation we are looking for.

3.2.1 Fourier Transform of the Hamiltonian

The Hamiltonian in Eq. (3.8) contains two different operators which act on two different sub-lattices. To simplify our problem, we distinguish the creation as well as the annihilation operator between the sub-lattices they are acting on. We use the Fourier transform in Eq. (2.13) and transform the operators $c_{s,\,\vec{x}}$ and $c^\dagger_{s,\,\vec{x}}$ from position space into momentum space. For sub-lattice A, we obtain

$$\tilde{c}_{s,A}(\vec{k}) = \sum_{\vec{x}\in X_A} c_{s,\,\vec{x}} \exp(-i\vec{k}\cdot\vec{x}) = \exp(-i\vec{k}\cdot\vec{e}_A) \sum_{\vec{x}\in X} c_{s,\,\vec{x}+\vec{e}_A} \exp(-i\vec{k}\cdot\vec{x}), \tag{3.9}$$

$$\tilde{c}_{s,A}(\vec{k})^\dagger = \sum_{\vec{x}\in X_A} c^\dagger_{s,\,\vec{x}} \exp(i\vec{k}\cdot\vec{x}) = \exp(i\vec{k}\cdot\vec{e}_A) \sum_{\vec{x}\in X} c^\dagger_{s,\,\vec{x}+\vec{e}_A} \exp(i\vec{k}\cdot\vec{x}), \tag{3.10}$$

and in a similar way for the sub-lattice B, we obtain

$$\tilde{c}_{s,B}(\vec{k}) = \exp(-i\vec{k}\cdot\vec{e}_B) \sum_{\vec{x}\in X} c_{s,\,\vec{x}+\vec{e}_B} \exp(-i\vec{k}\cdot\vec{x}), \tag{3.11}$$

$$\tilde{c}_{s,B}(\vec{k})^\dagger = \exp(i\vec{k}\cdot\vec{e}_B) \sum_{\vec{x}\in X} c^\dagger_{s,\,\vec{x}+\vec{e}_B} \exp(i\vec{k}\cdot\vec{x}). \tag{3.12}$$

The inverse Fourier transform, which is constructed in Eq. (2.19), finally yields four different expression. We obtain for each sub-lattice a creation and an annihilation operator, which are given by

$$\begin{aligned} c_{s,\,\vec{x}+\vec{e}_A} &= \frac{\sqrt{3}\,a^2}{8\pi^2} \int_B d^2k\, \tilde{c}_{s,A}(\vec{k}) \exp(i\vec{k}\cdot(\vec{x}+\vec{e}_A)), \\ c^\dagger_{s,\,\vec{x}+\vec{e}_A} &= \frac{\sqrt{3}\,a^2}{8\pi^2} \int_B d^2k\, \tilde{c}_{s,A}(\vec{k})^\dagger \exp(-i\vec{k}\cdot(\vec{x}+\vec{e}_A)), \\ c_{s,\,\vec{x}+\vec{e}_B} &= \frac{\sqrt{3}\,a^2}{8\pi^2} \int_B d^2k\, \tilde{c}_{s,B}(\vec{k}) \exp(i\vec{k}\cdot(\vec{x}+\vec{e}_B)), \\ c^\dagger_{s,\,\vec{x}+\vec{e}_B} &= \frac{\sqrt{3}\,a^2}{8\pi^2} \int_B d^2k\, \tilde{c}_{s,B}(\vec{k})^\dagger \exp(-i\vec{k}\cdot(\vec{x}+\vec{e}_B)). \end{aligned} \tag{3.13}$$

With the four relations above, we can finally transform the Hamiltonian in Eq. (3.8) from position space into momentum space. We obtain the Hamiltonian in momentum space, which is given by

$$\begin{aligned}\mathcal{H} = -t \sum_{\vec{x},s} \left(\frac{\sqrt{3}\, a^2}{8\pi^2} \right)^2 \int_B d^2k \int_B d^2k' \\ \Big[\tilde{c}_{s,B}(\vec{k})^\dagger \tilde{c}_{s,A}(\vec{k}') \exp\left(i(\vec{k}' \cdot (\vec{x} + \vec{e}_A) - \vec{k} \cdot (\vec{x} + \vec{e}_B + \vec{a}_1)) \right) \\ + \tilde{c}_{s,A}(\vec{k})^\dagger \tilde{c}_{s,B}(\vec{k}') \exp\left(i(\vec{k}' \cdot (\vec{x} + \vec{e}_B + \vec{a}_2) - \vec{k} \cdot (\vec{x} + \vec{e}_A)) \right) \\ + \tilde{c}_{s,B}(\vec{k})^\dagger \tilde{c}_{s,A}(\vec{k}') \exp\left(i(\vec{k}' \cdot (\vec{x} + \vec{e}_A - \vec{a}_1) - \vec{k} \cdot (\vec{x} + \vec{e}_B + \vec{a}_2)) \right) \\ + \tilde{c}_{s,A}(\vec{k})^\dagger \tilde{c}_{s,B}(\vec{k}') \exp\left(i(\vec{k}' \cdot (\vec{x} + \vec{e}_B) - \vec{k}\, (\vec{x} + \vec{e}_A - \vec{a}_1)) \right) \\ + \tilde{c}_{s,B}(\vec{k})^\dagger \tilde{c}_{s,A}(\vec{k}') \exp\left(i(\vec{k}' \cdot (\vec{x} + \vec{e}_A - \vec{a}_2) - \vec{k} \cdot (\vec{x} + \vec{e}_B)) \right) \\ + \tilde{c}_{s,A}(\vec{k})^\dagger \tilde{c}_{s,B}(\vec{k}') \exp\left(i(\vec{k}' \cdot (\vec{x} + \vec{e}_B + \vec{a}_1) - \vec{k} \cdot (\vec{x} + \vec{e}_A - \vec{a}_2)) \right) \Big]. \end{aligned} \tag{3.14}$$

In Eq. (3.14) above, one of the two integrations can be performed using the δ-function which was constructed in Eq. (2.23). By simplifying the expression, we are able to identify the δ-function $\delta(\vec{k}' - \vec{k})$, i.e. we obtain

$$\begin{aligned}\mathcal{H} = -t \sum_{s} \left(\frac{\sqrt{3}\, a^2}{8\pi^2} \right) \int_B d^2k \int_B d^2k' \underbrace{\left(\frac{\sqrt{3}\, a^2}{8\pi^2} \right) \sum_{\vec{x}} \exp\left(i\vec{x} \cdot (\vec{k}' - \vec{k}) \right)}_{\delta(\vec{k}' - \vec{k})} \\ \Big[\tilde{c}_{s,B}(\vec{k})^\dagger \tilde{c}_{s,A}(\vec{k}') \exp\left(i(\vec{k}' \cdot \vec{e}_A - \vec{k} \cdot (\vec{e}_B + \vec{a}_1)) \right) \\ + \tilde{c}_{s,A}(\vec{k})^\dagger \tilde{c}_{s,B}(\vec{k}') \exp\left(i(\vec{k}' \cdot (\vec{e}_B + \vec{a}_2) - \vec{k} \cdot \vec{e}_A) \right) \\ + \tilde{c}_{s,B}(\vec{k})^\dagger \tilde{c}_{s,A}(\vec{k}') \exp\left(i(\vec{k}' \cdot (\vec{e}_A - \vec{a}_1) - \vec{k} \cdot (\vec{e}_B + \vec{a}_2)) \right) \\ + \tilde{c}_{s,A}(\vec{k})^\dagger \tilde{c}_{s,B}(\vec{k}') \exp\left(i(\vec{k}' \cdot \vec{e}_B - \vec{k} \cdot (\vec{e}_A - \vec{a}_1)) \right) \\ + \tilde{c}_{s,B}(\vec{k})^\dagger \tilde{c}_{s,A}(\vec{k}') \exp\left(i(\vec{k}' \cdot (\vec{e}_A - \vec{a}_2) - \vec{k} \cdot \vec{e}_B) \right) \\ + \tilde{c}_{s,A}(\vec{k})^\dagger \tilde{c}_{s,B}(\vec{k}') \exp\left(i(\vec{k}' \cdot (\vec{e}_B + \vec{a}_1) - \vec{k} \cdot (\vec{e}_A - \vec{a}_2)) \right) \Big], \end{aligned} \tag{3.15}$$

and can simplify the Hamiltonian to

$$\begin{aligned}\mathcal{H} = -t \sum_{s} \left(\frac{\sqrt{3}\, a^2}{8\pi^2} \right) \int_B d^2k \\ \Big[\tilde{c}_{s,B}(\vec{k})^\dagger \tilde{c}_{s,A}(\vec{k}) \exp\left(i\vec{k} \cdot (\vec{e}_A - \vec{e}_B - \vec{a}_1) \right) \\ + \tilde{c}_{s,A}(\vec{k})^\dagger \tilde{c}_{s,B}(\vec{k}) \exp\left(i\vec{k} \cdot (\vec{e}_B + \vec{a}_2 - \vec{e}_A) \right) \\ + \tilde{c}_{s,B}(\vec{k})^\dagger \tilde{c}_{s,A}(\vec{k}) \exp\left(i\vec{k} \cdot (\vec{e}_A - \vec{a}_1 - \vec{e}_B - \vec{a}_2) \right) \\ + \tilde{c}_{s,A}(\vec{k})^\dagger \tilde{c}_{s,B}(\vec{k}) \exp\left(i\vec{k} \cdot (\vec{e}_B - \vec{e}_A + \vec{a}_1) \right) \\ + \tilde{c}_{s,B}(\vec{k})^\dagger \tilde{c}_{s,A}(\vec{k}) \exp\left(i\vec{k} \cdot (\vec{e}_A - \vec{a}_2 - \vec{e}_B) \right) \\ + \tilde{c}_{s,A}(\vec{k})^\dagger \tilde{c}_{s,B}(\vec{k}) \exp\left(i\vec{k} \cdot (\vec{e}_B + \vec{a}_1 - \vec{e}_A + \vec{a}_2) \right) \Big]. \end{aligned} \tag{3.16}$$

With Eq. (2.7), we obtain

$$\begin{aligned}\mathcal{H} = -t\sum_s \left(\frac{\sqrt{3}\,a^2}{8\pi^2}\right)\int_B d^2k \\ \Big[&\tilde{c}_{s,B}(\vec{k})^\dagger \tilde{c}_{s,A}(\vec{k}) \exp\big(-i\vec{k}\cdot\vec{a}_1\big)\exp\big(-2i\,\vec{k}\cdot\vec{e}_A\big) \\ &+\tilde{c}_{s,A}(\vec{k})^\dagger \tilde{c}_{s,B}(\vec{k}) \exp\big(i\vec{k}\cdot\vec{a}_2\big)\exp\big(2i\,\vec{k}\cdot\vec{e}_A\big) \\ &+\tilde{c}_{s,B}(\vec{k})^\dagger \tilde{c}_{s,A}(\vec{k}) \exp\big(-i\vec{k}\cdot(\vec{a}_1+\vec{a}_2)\big)\exp\big(-2i\,\vec{k}\cdot\vec{e}_A\big) \\ &+\tilde{c}_{s,A}(\vec{k})^\dagger \tilde{c}_{s,B}(\vec{k}) \exp\big(i\vec{k}\cdot\vec{a}_1\big)\exp\big(2i\,\vec{k}\cdot\vec{e}_A\big) \\ &+\tilde{c}_{s,B}(\vec{k})^\dagger \tilde{c}_{s,A}(\vec{k}) \exp\big(-i\vec{k}\cdot\vec{a}_2\big)\exp\big(-2i\,\vec{k}\cdot\vec{e}_A\big) \\ &+\tilde{c}_{s,A}(\vec{k})^\dagger \tilde{c}_{s,B}(\vec{k}) \exp\big(i\vec{k}\cdot(\vec{a}_1+\vec{a}_2)\big)\exp\big(2i\,\vec{k}\cdot\vec{e}_A\big)\Big],\end{aligned} \tag{3.17}$$

and are finally able to simplify the Hamiltonian in momentum space

$$\mathcal{H} = -t\sum_s \left(\frac{\sqrt{3}\,a^2}{8\pi^2}\right)\int_B d^2k\Big(\epsilon(\vec{k})^*\tilde{c}_{s,B}(\vec{k})^\dagger\tilde{c}_{s,A}(\vec{k}) + \epsilon(\vec{k})\,\tilde{c}_{s,A}(\vec{k})^\dagger\tilde{c}_{s,B}(\vec{k})\Big). \tag{3.18}$$

where we have introduced a phase factor $\epsilon(\vec{k})$, defined by

$$\epsilon(\vec{k}) := \exp(2i\,\vec{k}\,\vec{e}_A)\big[\exp(i\vec{k}\,\vec{a}_1) + \exp(i\vec{k}\,\vec{a}_2) + \exp(i\vec{k}\,(\vec{a}_1+\vec{a}_2))\big]. \tag{3.19}$$

By using the Fourier transform, which was derived in chapter 2, we have finally obtained a simple form of the Hamiltonian $\mathcal{H}$ in Eq. (3.18) together with the phase factor $\epsilon(\vec{k})$ in Eq. (3.19).

3.2.2 Diagonalization

The distinction of different creation as well as annihilation operators at the beginning of the previous section 3.2.1 generates a two-component spinor in the Hamiltonian $\mathcal{H}$ which represents the sub-lattices A and B. For this reason, we rewrite $\mathcal{H}$ in matrix representation and obtain

$$\mathcal{H} = -\,t\sum_s \left(\frac{\sqrt{3}\,a^2}{8\pi^2}\right)\int_B d^2k\Big(\tilde{c}_{s,A}(\vec{k})^\dagger,\,\tilde{c}_{s,B}(\vec{k})^\dagger\Big)\begin{pmatrix}0 & \epsilon(\vec{k})\\ \epsilon^*(\vec{k}) & 0\end{pmatrix}\begin{pmatrix}\tilde{c}_{s,A}(\vec{k})\\ \tilde{c}_{s,B}(\vec{k})\end{pmatrix}. \tag{3.20}$$

To extract the dispersion relation $E(\vec{k})$, we have to diagonalize the Hamiltonian $\mathcal{H}$. The only non-diagonal term in Eq. (3.20) is the two-dimensional quadratic matrix which contains the phase factor $\epsilon(\vec{k})$, i.e. we define

$$A := \begin{pmatrix}0 & \epsilon(\vec{k})\\ \epsilon^*(\vec{k}) & 0\end{pmatrix} \in U(2) = \{A \in Mat(2\times 2,\mathbb{C}) | A^\dagger A = E_2\}. \tag{3.21}$$

The matrix A is a unitary matrix by definition. For this reason, we have to find a matrix $U \in U(2)$ generated by the eigenvectors of A, such that we can diagonalize A with it, i.e.

$$D = U\,A\,U^\dagger. \tag{3.22}$$

A possible unitary transformation with a matrix U is given by

$$U := \frac{1}{\sqrt{2}} \begin{pmatrix} \exp(i\frac{\alpha}{2}) & \exp(-i\frac{\alpha}{2}) \\ \exp(i\frac{\alpha}{2}) & -\exp(-i\frac{\alpha}{2}) \end{pmatrix} \in U(2). \tag{3.23}$$

With Eq. (3.22) and Eq. (3.23), we are able to diagonalize the matrix A in Eq. (3.21) and obtain

$$\begin{aligned} U \begin{pmatrix} 0 & \epsilon(\vec{k}) \\ \epsilon^*(\vec{k}) & 0 \end{pmatrix} U^\dagger &= \begin{pmatrix} \exp(i\frac{\alpha}{2}) & \exp(-i\frac{\alpha}{2}) \\ \exp(i\frac{\alpha}{2}) & -\exp(-i\frac{\alpha}{2}) \end{pmatrix} \begin{pmatrix} 0 & \epsilon(\vec{k}) \\ \epsilon^*(\vec{k}) & 0 \end{pmatrix} \begin{pmatrix} \exp(-i\frac{\alpha}{2}) & \exp(-i\frac{\alpha}{2}) \\ \exp(i\frac{\alpha}{2}) & -\exp(i\frac{\alpha}{2}) \end{pmatrix} \\ \implies U \begin{pmatrix} 0 & \epsilon(\vec{k}) \\ \epsilon^*(\vec{k}) & 0 \end{pmatrix} U^\dagger &= \begin{pmatrix} |\epsilon(\vec{k})| & 0 \\ 0 & -|\epsilon(\vec{k})| \end{pmatrix}. \end{aligned} \tag{3.24}$$

With Eq. (3.24), the matrix A in diagonal form, the Hamiltonian $\mathcal{H}$ in Eq. (3.20) finally reduces to

$$\mathcal{H} = -\,t \sum_s \left(\frac{\sqrt{3}\,a^2}{8\pi^2} \right) \int_B d^2k \big(\tilde{c}_{s,A}(\vec{k})^\dagger,\, \tilde{c}_{s,B}(\vec{k})^\dagger \big)\, U^\dagger \begin{pmatrix} |\epsilon(\vec{k})| & 0 \\ 0 & -|\epsilon(\vec{k})| \end{pmatrix} U \begin{pmatrix} \tilde{c}_{s,A}(\vec{k}) \\ \tilde{c}_{s,B}(\vec{k}) \end{pmatrix}. \tag{3.25}$$

In Eq. (3.25) above we have obtained an expression for $\mathcal{H}$ which contains only diagonal terms. For this reason, we are able to extract the dispersion relation $E(\vec{k})$ in the following section 3.2.3.

3.2.3 Dispersion Relation

By considering the eigenvalue equation $\mathcal{H}\,\psi = E\,\psi$ and the Hamiltonian $\mathcal{H}$ in Eq. (3.25), we see that the information about the energy of the electrons on the graphene lattice is encoded in the absolute value of the phase factor $\epsilon(\vec{k})$ in combination with the hopping parameter t. Therefore, we finally obtain the dispersion relation which is given by

$$E_\pm(\vec{k}) = \pm\, t\, |\epsilon(\vec{k})|. \tag{3.26}$$

In order to visualize the dispersion relation, we simplify the expression $|\epsilon(\vec{k})|$ where the phase factor $\epsilon(\vec{k})$ is given in Eq. (3.19). Using the primitive vectors $\vec{a}_1$ and $\vec{a}_2$ in Eq. (2.1), we obtain

$$\begin{aligned} |\epsilon(\vec{k})|^2 &= \epsilon(\vec{k})\epsilon(\vec{k})^* \\ &= [\exp(i\,\vec{k}\cdot\vec{a}_1) + \exp(i\,\vec{k}\cdot\vec{a}_2) + \exp(i\,\vec{k}\cdot(\vec{a}_1+\vec{a}_2))] \\ &\times [\exp(-i\,\vec{k}\cdot\vec{a}_1) + \exp(-i\,\vec{k}\cdot\vec{a}_2) + \exp(-i\,\vec{k}\cdot(\vec{a}_1+\vec{a}_2))] \\ &= 3 + 2\cosh(i\,\vec{k}\cdot\vec{a}_1) + 2\cosh(i\,\vec{k}\cdot\vec{a}_2) + 2\cosh(i\cdot\vec{k}\,(\vec{a}_1-\vec{a}_2)) \\ &= 3 + 2\cos(\vec{k}\cdot\vec{a}_1) + 2\cos(\vec{k}\cdot\vec{a}_2) + 2\cos(\vec{k}\cdot(\vec{a}_1-\vec{a}_2)) \\ &= 3 + 2\cos(2\pi\,m_1) + 2\cos(2\pi\,m_2) + 2\cos(2\pi\,(m_1-m_2)), \end{aligned} \tag{3.27}$$

represented in the basis $\{\vec{b}_1, \vec{b}_2\}$ (see Eq. 2.17). With the relation between the parameters m_1, m_2 and k_x, k_y, as shown in Eq. (2.20), the absolute value squared becomes

$$\begin{aligned} |\epsilon(\vec{k})|^2 &= 3 + 2\cos(\frac{a}{2}k_x) + 2\cos(\frac{\sqrt{3}\,a}{2}k_y + \frac{a}{2}k_x) + 2\cos(\frac{a}{2}k_1 - \frac{\sqrt{3}a}{2}k_2) \\ &= 3 + 2\cos(a\,k_x) + 4\cos(\frac{a}{2}k_x)\cos(\frac{\sqrt{3}\,a}{2}k_y). \end{aligned} \tag{3.28}$$

After all, we find a dispersion relation which is given by

$$E_{\pm}(\vec{k}) = \pm t\,|\epsilon(\vec{k})| = \pm t\sqrt{3 + 2\cos(a\,k_x) + 4\cos(\frac{a}{2}k_x)\cos(\frac{\sqrt{3}\,a}{2}k_y)}, \tag{3.29}$$

represented in the orthogonal basis $\{k_x, k_y\}$. This result is completely symmetric around the center Γ of the first Brillouin zone. By referring to the plus-minus sign in Eq. (3.29), the dispersion relation forms two identical bands of allowed energy states, namely the upper conduction and the lower valence band which are illustrated in Fig. 3.1.

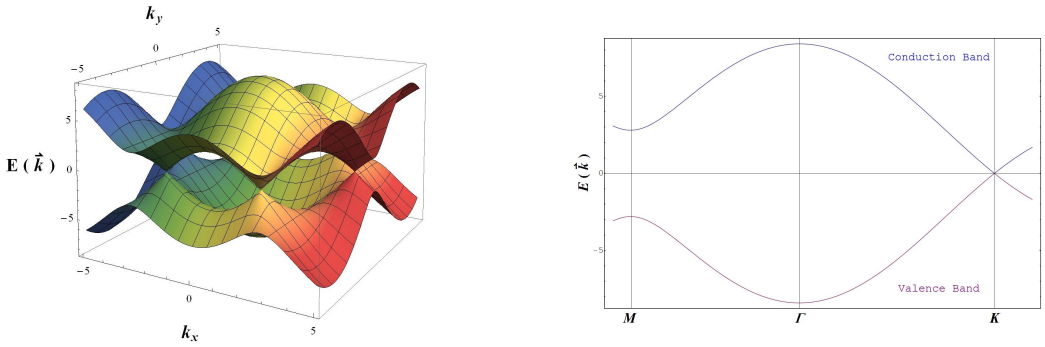

Figure 3.1: In both figures, the dispersion relation $E(\vec{k})$ is shown limited on the first Brillouin zone for a value $t = 2.8eV$. On the left, the full energy spectrum of graphene is illustrated in 3D ($[k_x] = [k_y] = \frac{1}{a}$ and $\left[E(\vec{k})\right] = eV$). On the right, $E(\vec{k})$ expresses the symmetry between the conduction and valence band by introducing the points of high symmetry, namely M, Γ and K.

By considering the dispersion relation more in detail, we observe that the value of the hopping parameter t determines the energy scale but not the shape of $E(\vec{k})$. In addition, the dispersion relation determines the so-called Fermi surface which consist of six different zero points, the six Dirac points which are mentioned in section 2.2, i.e. in Eq. (2.10) and in Eq. (2.11). The corresponding Fermi level E_F lies between the two symmetrical bands. Through this connection of these bands in points of $E = E_F = 0$, graphene shows a semi-metallic behavior which can be interpreted as a zero-gap semiconductor. Note that semiconductors are strongly dependent on temperature. We are talking about a half-filled ground state, when all states in the lower valence band $E_-(\vec{k})$ are occupied, while the states in the upper conduction band $E_+(\vec{k})$ are completely empty. This is the case in the absolute zero point $T = 0$ and graphene becomes an insulator. In the following chapter 4, we will discuss the Dirac points in more detail by expanding the dispersion relation around them in order to obtain an effective low-energy description.

3.3 Electron Hopping to Next-to-Nearest Neighbors

To conclude this chapter 3, we extend the Hamiltonian in Eq. (3.7), i.e. we consider electron hopping to nearest-and next-to-nearest-neighbor ions. Hence, the electrons are allowed to hop from one sub-lattice to another or to hop onto the same again. Therefore, the extended Hamiltonian is a sum of the Hamiltonian in Eq. (3.7) and a Hamiltonian which describes

electron hopping between next-to-nearest-neighbor ions. We obtain

$$\mathcal{H}+\mathcal{H}' = -t \sum_{\substack{<\vec{x},\vec{y}> \\ s=\uparrow,\downarrow}} \left(c^\dagger_{\vec{x}} c_{\vec{y}} + c^\dagger_{\vec{y}} c_{\vec{x}} \right) - t' \sum_{\substack{<<\vec{x},\vec{y}>> \\ s=\uparrow,\downarrow}} \left(c^\dagger_{\vec{x}} c_{\vec{y}} + c^\dagger_{\vec{y}} c_{\vec{x}} \right), \tag{3.30}$$

where we have introduced another hopping parameter t' for which in general $t' \neq t$. We have already solved the Hamiltonian $\mathcal{H}$ in Eq. (3.25), so we only have to concentrate us on the additional Hamiltonian $\mathcal{H}'$ by diagonalizing the sum $\mathcal{H}+\mathcal{H}'$ as we see later. However, first we have to formulate the Hamiltonian term $\mathcal{H}'$ in Eq. (3.30) for electron hopping to next-to-nearest-neighbors like in Eq. (3.7) for the Hamiltonian $\mathcal{H}$ and obtain

$$\begin{aligned}
\mathcal{H}' = -t' \sum_{\vec{x},s} \Big[& c^\dagger_{s,\,\vec{x}+\vec{e}_A-\vec{a}_2}\, c_{s,\,\vec{x}+\vec{e}_A} + c^\dagger_{s,\,\vec{x}+\vec{e}_A}\, c_{s,\,\vec{x}+\vec{e}_A-\vec{a}_2} \\
& + c^\dagger_{s,\,\vec{x}+\vec{e}_A-\vec{a}_1}\, c_{s,\,\vec{x}+\vec{e}_A-\vec{a}_2} + c^\dagger_{s,\,\vec{x}+\vec{e}_A-\vec{a}_2}\, c_{s,\,\vec{x}+\vec{e}_A-\vec{a}_1} \\
& + c^\dagger_{s,\,\vec{x}+\vec{e}_A}\, c_{s,\,\vec{x}+\vec{e}_A-\vec{a}_1} + c^\dagger_{s,\,\vec{x}+\vec{e}_A-\vec{a}_1}\, c_{s,\,\vec{x}+\vec{e}_A} \\
& + c^\dagger_{s,\vec{x}+\vec{e}_B+\vec{a}_1}\, c_{s\,\vec{x}+\vec{e}_B+\vec{a}_2} + c^\dagger_{s,\,\vec{x}+\vec{e}_B+\vec{a}_2}\, c_{s,\,\vec{x}+\vec{e}_B+\vec{a}_1} \\
& + c^\dagger_{s,\,\vec{x}+\vec{e}_B}\, c_{s,\,\vec{x}+\vec{e}_B+\vec{a}_1} + c^\dagger_{s,\,\vec{x}+\vec{e}_B+\vec{a}_1}\, c_{s\,\vec{x}+\vec{e}_B} \\
& + c^\dagger_{s,\,\vec{x}+\vec{e}_B+\vec{a}_2}\, c_{s,\,\vec{x}+\vec{e}_B} + c^\dagger_{s,\,\vec{x}+\vec{e}_B}\, c_{s,\vec{x}+\vec{e}_B+\vec{a}_2} \Big].
\end{aligned} \tag{3.31}$$

In analogy to the Hamiltonian $\mathcal{H}$ in Eq. (3.18), the expression for $\mathcal{H}'$ above in Eq. (3.31) can be simplified to the compact form

$$\mathcal{H}' = -\,t' \sum_s \left(\frac{\sqrt{3}\,a^2}{8\pi^2} \right) \int_B d^2k \Big(\kappa(\vec{k}) \tilde{c}_{s,B}(\vec{k})^\dagger \tilde{c}_{s,A}(\vec{k}) + \kappa(\vec{k})\, \tilde{c}_{s,A}(\vec{k})^\dagger \tilde{c}_{s,B}(\vec{k}) \Big), \tag{3.32}$$

where we have defined a new phase factor $\kappa(\vec{k})$ given by

$$\begin{aligned}
\kappa(\vec{k}) = {} & \exp(i\,\vec{k}\cdot\vec{a}_1) + \exp(i\,\vec{k}\cdot\vec{a}_2) + \exp(i\,\vec{k}\cdot(\vec{a}_2-\vec{a}_1)) \\
& + \exp(-i\,\vec{k}\cdot\vec{a}_1) + \exp(-i\,\vec{k}\cdot\vec{a}_2) + \exp(-i\,\vec{k}\cdot(\vec{a}_2-\vec{a}_1)).
\end{aligned} \tag{3.33}$$

At this point of development, we already simplify the new phase factor $\kappa(\vec{k})$ in the basis of $\{k_x, k_y\}$, i.e. we obtain

$$\begin{aligned}
\kappa(\vec{k}) &= 2\cos(\vec{k}\cdot\vec{a}_1) + 2\cos(\vec{k}\cdot\vec{a}_2) + 2\cos(\vec{k}\cdot(\vec{a}_2-\vec{a}_1)) \\
&= 2\cos(a\,k_x) + 4\cos(\frac{a}{2}k_x)\cos(\frac{\sqrt{3}\,a}{2}k_y).
\end{aligned} \tag{3.34}$$

Finally, using Eq. (3.18) and (3.32), we can rewrite the Hamiltonian in Eq. (3.30) in matrix representation and obtain

$$\mathcal{H}+\mathcal{H}' = -\sum_s \left(\frac{\sqrt{3}\,a^2}{8\pi^2} \right) \int_B d^2k \big(\tilde{c}_{s,A}(\vec{k})^\dagger,\, \tilde{c}_{s,B}(\vec{k})^\dagger \big) \begin{pmatrix} t'\,\kappa(\vec{k}) & t\,\epsilon(\vec{k}) \\ t\,\epsilon^*(\vec{k}) & t'\,\kappa(\vec{k}) \end{pmatrix} \begin{pmatrix} \tilde{c}_{s,A}(\vec{k}) \\ \tilde{c}_{s,B}(\vec{k}) \end{pmatrix}. \tag{3.35}$$

With the same unitary matrix U in Eq. (3.23), we are able to diagonalize the Hamiltonian in Eq. (3.35) above and obtain

$$\mathcal{H}+\mathcal{H}' = -\sum_s \left(\frac{\sqrt{3}\,a^2}{8\pi^2}\right)\int_B d^2k \times \left(\tilde{c}_{s,A}(\vec{k})^\dagger,\, \tilde{c}_{s,B}(\vec{k})^\dagger\right) U \begin{pmatrix} t'\,\kappa(\vec{k}) + t\,|\epsilon(\vec{k})| & 0 \\ 0 & t'\,\kappa(\vec{k}) - t\,|\epsilon(\vec{k})| \end{pmatrix} U^\dagger \begin{pmatrix} \tilde{c}_{s,A}(\vec{k}) \\ \tilde{c}_{s,B}(\vec{k}) \end{pmatrix}, \tag{3.36}$$

where we can extract the dispersion relation for the extended Hamiltonian $\mathcal{H}+\mathcal{H}'$ as

$$E_\pm(\vec{k}) = \pm t\,|\epsilon(\vec{k})| - t'\,\kappa(\vec{k}) = \pm t\,\sqrt{3+f(\vec{k})} - t'\,f(\vec{k}), \tag{3.37}$$

by introducing a new phase factor $f(\vec{k})$ which is given by

$$f(\vec{k}) = 2\cos(a\,k_x) + 4\cos(\frac{a}{2}k_x)\cos(\frac{\sqrt{3}\,a}{2}k_y). \tag{3.38}$$

The additional Hamiltonian $\mathcal{H}'$ generates an additional term in the dispersion relation $E(\vec{k})$, and the two different phase factors $\epsilon(\vec{k})$ and $\kappa(\vec{k})$ merge to a new phase factor $f(\vec{k})$. With $t'=0$, the dispersion relation stays symmetric as in Fig. 3.1. However, if $t'\neq 0$, we obtain an asymmetry between conduction and valence band (see Fig 3.2).

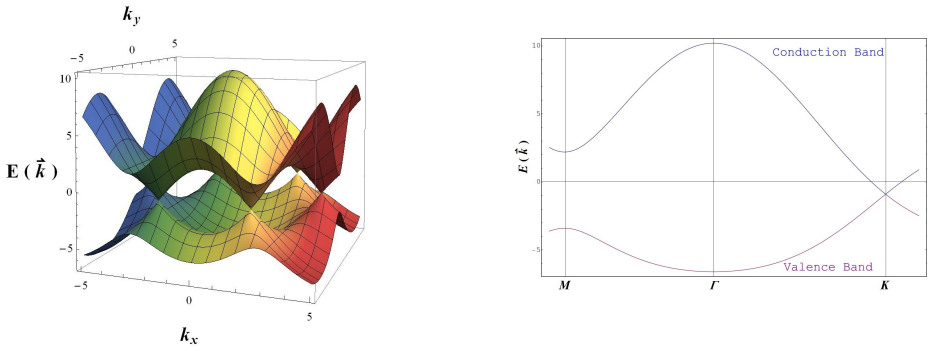

Figure 3.2: The dispersion relation of the extended Hamiltonian $\mathcal{H}+\mathcal{H}'$ is illustrated in 3D on the left and in 2D with introduced points of high symmetry on the right (with $t = 2.8eV$ and $t' = 0.1eV$ [7]). The value of t' is the result obtained in cyclotron resonance experiment[12].

By referring to the work of S. Reich *Tight-binding description of graphene*[13], the inclusion of electron hopping to second- as well as third-nearest-neighbors yield a more precise thigh-binding approximation. The dispersion relation in Eq. (3.29) predicts the electric energy only for a finite range of wave vector $\vec{k}$ whereas the extended dispersion in Eq. (3.37) quite accurately describes energy states $E(\vec{k})$ over the whole first Brillouin zone. By comparing both dispersion relations in detail, we observe in the second dispersion relation in Eq. (3.37) a certain electron-hole asymmetry due to the energy shift of the Dirac points, as we see in Fig. 3.2. Unfortunately, we would go beyond the scope of this thesis by considering this aspect of asymmetry in more detail. Therefore, we mention it here for completeness.

Chapter 4

Effective Low-Energy Description

A very interesting aspect of Graphene is the low-energy description using an effective theory. For this purpose, we consider at the connection of the upper conduction and the lower valence band, i.e. at the vicinity of the Dirac points K and K'. When we expand the dispersion relation around these points, we obtain in first order approximation a linear characteristic. For small energy the dispersion relation forms so-called Dirac cones. The existence of these cones implies that Graphene is classified as a conventional semiconductor, because there is no gap between conduction and valence band. The mentioned interesting aspect arises when we consider the Fermi velocity v_F. In fact, Graphene's low-energy excitations are relativistic, massless, quasi-free Dirac fermions which are moving through the honeycomb lattice with a velocity v_F. Between the Fermi velocity v_F and the speed of light c, there is a factor 300[7]. Due to this reduced speed of light, many unusual properties of quantum electrodynamics (QED) can be discussed in Graphene at much smaller speeds. In addition, Graphene, with such a high Fremi velocity, shows its high quality as a conductor of electricity.
In this chapter 4, we first acquaint ourselves with the interacting fermions as Dirac fermions. In a second step, we develop an effective theory for small energies based on the Dirac equation. We discuss Dirac points, cones and fermions in graphene, because we use the relativistic variant of the Schrödinger equation, the mentioned Dirac equation, for describing the low-energy dynamics. Furthermore, the results of this chapter 4 are essential for describing in chapter 5 some properties of graphene in an external magnetic field, because, in comparison with ordinary electrons, Dirac fermions behave in an unusual manner.

4.1 Dirac Cones

At the beginning of section 2.2, we have highlighted the Dirac points as the six corners of the first Brillouin zone and have chosen one Dirac point K and K' in Eq. (2.12). Obviously, all further calculations concerning these Dirac cones are analytically identical.
We start by expanding the dispersion relation in Eq. (3.29) around the Dirac point K for an infinitesimal vector $\Delta\vec{k}$. With the first and second order derivatives of $|\epsilon(\vec{k})|^2$

$$\frac{\partial|\epsilon(\vec{k})|^2}{\partial k_x} = -2\,a\sin(a\,k_x) - 2a\sin(\frac{a}{2}\,k_x)\cos(\frac{\sqrt{3}\,a}{2}\,k_y), \tag{4.1}$$

$$\frac{\partial|\epsilon(\vec{k})|^2}{\partial k_y} = -2\sqrt{3}\,a\cos(\frac{a}{2}\,k_x)\sin(\frac{\sqrt{3}\,a}{2}\,k_y), \tag{4.2}$$

$$\frac{\partial^2|\epsilon(\vec{k})|^2}{\partial k_x^2} = -2\,a^2\cos(a\,k_x) - a^2\cos(\frac{a}{2}\,k_x)\cos(\frac{\sqrt{3}\,a}{2}\,k_y), \tag{4.3}$$

$$\frac{\partial^2|\epsilon(\vec{k})|^2}{\partial k_y^2} = -3\,a^2\cos(\frac{a}{2}\,k_x)\cos(\frac{\sqrt{3}\,a}{2}\,k_y), \tag{4.4}$$

$$\frac{\partial^2|\epsilon(\vec{k})|^2}{\partial k_x \partial k_y} = \sqrt{3}\,a^2\sin(\frac{a}{2}\,k_x)\sin(\frac{\sqrt{3}\,a}{2}\,k_y), \tag{4.5}$$

we evaluate the expansion to second order

$$\begin{aligned}|\epsilon(\vec{k}+\Delta\vec{k})|^2 =& |\epsilon(\vec{k})|^2\Big|_{\vec{k}=K} + \frac{\partial|\epsilon(\vec{k})|^2}{\partial k_x}\Big|_{\vec{k}=K}\Delta k_x + \frac{\partial|\epsilon(\vec{k})|^2}{\partial k_y}\Big|_{\vec{k}=K}\Delta k_y \\ &+ \frac{1}{2}\left[\frac{\partial^2|\epsilon(\vec{k})|^2}{\partial k_x^2}\Big|_{\vec{k}=K}\Delta k_x^2 + \frac{\partial^2|\epsilon(\vec{k})|^2}{\partial k_x^2}\Big|_{\vec{k}=K}\Delta k_x^2 + 2\frac{\partial^2|\epsilon(\vec{k})|^2}{\partial k_x \partial k_y}\Big|_{\vec{k}=K}\Delta k_x\,\Delta k_x\right] + \mathcal{O}(\vec{k}^3),\end{aligned} \tag{4.6}$$

around K and obtain

$$|\epsilon(K+\Delta\vec{k})|^2 = \frac{3}{4}a^2(\Delta k_x^2 + \Delta k_y^2) = \frac{3}{4}a^2|\Delta\vec{k}|^2. \tag{4.7}$$

Finally, the dispersion relation in first order approximation around K leads to

$$E_\pm(K+\Delta\vec{k}) = \pm t\,|\epsilon(K+\Delta\vec{k})| \approx \pm\frac{\sqrt{3}}{2}a\,t\,|\Delta\vec{k}| = \pm v_F\,\hbar\,|\Delta\vec{k}| = \pm v_F\,|\Delta\vec{p}|, \tag{4.8}$$

where v_F is the obtained Fermi velocity which is given by

$$v_F = \frac{\sqrt{3}}{2\hbar}a\,t. \tag{4.9}$$

By defining $\omega(\vec{k}) = v_F\,|\vec{k}|$, we obtain the usual compact form

$$E_\pm(K+\Delta\vec{k}) = \hbar\,\omega(K+\Delta\vec{k}). \tag{4.10}$$

As we see in Eq. (4.8) above, for small energies the dispersion relation forms the mentioned Dirac cones which arise in every Dirac point K and K', as shown in Fig. 4.1. Usually, the dispersion relation of massive particles has a parabolic form. Therefore, these cones are the first indicator of massless fermions in graphene. In addition, the Fermi velocity v_F, which we have extracted in Eq. (4.9), does depend on the hopping parameter t as well as on the lattice spacing a but has no dependence on the momentum $\vec{p}$. For massive particles on the Fermi surface, the Fermi momentum is related to the Fermi energy by

$$p_F = \sqrt{2\,m\,E_F}, \tag{4.11}$$

where the Fermi velocity is given by $v_F = \frac{dE}{dp}$. Therefore, we are talking about massless Dirac fermions in graphene given their behavior, i.e. we observe a linear dispersion relation around the Fermi level E_F and a Fermi velocity v_F which is independent on the Fermi momentum. When we include the results of section 3.3, the electron hopping to next-to-nearest-neighbors, we obtain in first order approximation the calculated linear term in Eq. (4.8) together with

additional terms of zeroth and second order. With the phase factor $\kappa(\vec{k})$ in first order approximation around the Dirac point K

$$\kappa(K + \Delta\vec{k}) \approx -3 + \frac{3}{4}a^2|\Delta\vec{k}|^2, \tag{4.12}$$

we obtain the approximated dispersion relation

$$E(K + \Delta\vec{k}) = \pm t\,|\epsilon(K + \Delta\vec{k})| - t'\,\kappa(K + \Delta\vec{k}) \approx -3t' + \frac{\sqrt{3}}{2}\,a\,t|\Delta\vec{k}| + \frac{3}{4}\,a^2\,t'\,|\Delta\vec{k}|^2. \tag{4.13}$$

The presence of an additional tunnelling parameter like t' breaks the electron-hole symmetry, as we have seen in section 3.3.

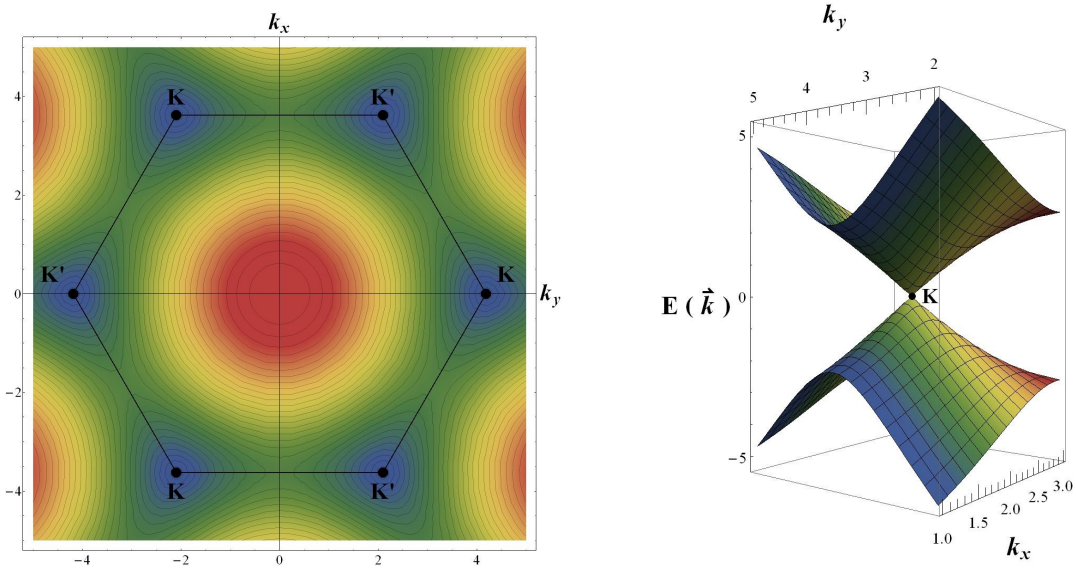

Figure 4.1: Left: Density plot of the dispersion relation $E(\vec{k})$ with indicated corners K and K' of the first Brillouin zone. Right: 3D illustration of a single Dirac cone. Both figures are based on the Hamiltonian $\mathcal{H}$ of electron hopping to nearest-neighbors with the dispersion relation of Eq. (3.29)

An immediate implication of this massless Dirac-like dispersion is a so-called cyclotron mass which depends on the electric charge density [7]. Therefore, this mass is measurable and provides evidence of the existence of massless Dirac quasi-free fermions in graphene.

4.2 Dirac Equation

In 1928, Dirac developed a relativistic form of the Schrödinger equation to describe relativistic electrons (fermions with spin $\frac{1}{2}$) and extended principles of quantum mechanic with elements of the special theory of relativity. Before Dirac's description, people believed in the Klein-Gordon equation as the only description. The only problem with it were their possible negative results for probability densities. Dirac was first to identify the problem with the second order time derivative and solved the problem with a time derivative of first order. Based on the Schrödinger equation, which consists of a time derivative of first order, Dirac developed the Dirac equation [14]. By considering the non-relativistic limit $\frac{v}{c} \to 0$, we obtain the Pauli

equation.
Relativistic quantum field theory as well as high-energy physics are based, among others, on the Dirac equation. In light of this, graphene shows the possibility of a non-relativistic application of Dirac's description (by referring to the low-non-relativistic energies).

4.2.1 Derivation and Connection to the Microscopic Model

For a possible alternative to the Klein-Gordon equation, we use the Schrödinger equation as an ansatz, i.e.

$$i\frac{\partial\psi}{\partial t} = \mathcal{H}_D\,\psi, \tag{4.14}$$

where in the case of graphene the wave function ψ describes electron states around the Dirac points K and K' (see section 4.2.3). Due to covariance, the Dirac-Hamiltonian in Eq. (4.14) has to consist of a space derivative of first order, i.e. we obtain Dirac's postulated Hamiltonian which is given by

$$\mathcal{H}_D = -i\,c\,\vec{\alpha}\cdot\vec{\nabla} + \beta\,m\,c^2 = \vec{\alpha}\cdot\vec{p}\,c + \beta\,m\,c^2, \tag{4.15}$$

where we still have to identify the quantities

$$\vec{\alpha} = \begin{pmatrix}\alpha_1\\ \alpha_2\\ \alpha_3\end{pmatrix}, \qquad \beta. \tag{4.16}$$

The Dirac equation then leads to

$$i\frac{\partial}{\partial t}\psi = (\vec{\alpha}\cdot\vec{p}\,c + \beta\,m\,c^2)\psi. \tag{4.17}$$

The unknown parameters have to conform to the relativistic energy-momentum relation $E^2 = (\vec{p}\,c)^2 + (m\,c^2)^2$, i.e. they have to conform to the relation

$$-\hbar^2\,\frac{\partial^2}{\partial\,t^2} = (\vec{\alpha}\,\vec{p}\,c + \beta\,m\,c^2)^2 = \vec{p}^{\,2}\,c^2 + (m\,c^2)^2, \tag{4.18}$$

which yields three conditions given by

$$\beta^2 = 1, \quad \vec{\alpha}\,\beta + \beta\,\vec{\alpha} = 0, \quad \alpha_i\,\alpha_j + \alpha_j\,\alpha_i = \delta_{ij}. \tag{4.19}$$

Dirac proved that the simplest form of $\vec{\alpha}$ and β is a 4×4 quadratic matrix. For their representation, there exists a number of well-known alternatives. As a possible solution of the conditions in Eq. (4.19) we have the Pauli-Dirac representation

$$\alpha_i = \begin{pmatrix}0 & \sigma_i\\ \sigma_i & 0\end{pmatrix}, \quad \beta = \begin{pmatrix}1 & 0\\ 0 & -1\end{pmatrix} = \begin{pmatrix}1 & 0 & 0 & 0\\ 0 & 1 & 0 & 0\\ 0 & 0 & -1 & 0\\ 0 & 0 & 0 & -1\end{pmatrix}, \tag{4.20}$$

or the Weyl representation

$$\alpha_i = \begin{pmatrix}-\sigma_i & 0\\ 0 & \sigma_i\end{pmatrix}, \quad \beta = \begin{pmatrix}0 & 1\\ 1 & 0\end{pmatrix}. \tag{4.21}$$

In both possible representations, we have used the Pauli matrices σ_i which are given by

$$\sigma_1 = \begin{pmatrix} 0 & 1 \\ 1 & 0 \end{pmatrix} \qquad \sigma_2 = \begin{pmatrix} 0 & -i \\ i & 0 \end{pmatrix} \qquad \sigma_3 = \begin{pmatrix} 1 & 0 \\ 0 & -1 \end{pmatrix}. \tag{4.22}$$

Before we start developing a Dirac equation in the case of massless fermions which are hopping on the graphene lattice (section 4.2.2), we have to identify the introduced operators of this section 4.2.1 with the observables from the previous section 4.1, such that we obtain comparable results. Taking the square of Eq. (4.8) yields

$$E_{\pm}(K + \Delta\vec{k}) = \frac{3}{4} a^2 \, t^2 |\Delta\vec{k}|^2. \tag{4.23}$$

By setting $m = 0$, $\vec{p} = \hbar\Delta\vec{k} = \hbar\,(\vec{k} - K)$ and $c = v_F$, the Dirac equation should show the same dispersion relation as the microscopic model, at least for small energies. The solutions are found by applying a Fourier transform

$$\psi(p, \omega) = \int_{-\infty}^{\infty} dt \, \psi(p, t) \, \exp(i \, \omega \, t). \tag{4.24}$$

The Dirac equation for $\psi(p, \omega)$ then states

$$(\hbar \, \omega - \sigma_i \, p_i \, c) \, \psi(p, \omega) = 0. \tag{4.25}$$

This implies that either $\psi(p, \omega) = 0$ or

$$det \, (\hbar \, \omega - \sigma_i \, p_i \, c) = det \begin{pmatrix} \hbar \, \omega & p_1 \, c - i \, p_2 \, c \\ p_1 \, c + i \, p_2 \, c & \hbar \, \omega \end{pmatrix} = (\hbar \, \omega)^2 - \vec{p}^2 \, c^2 = 0, \tag{4.26}$$

which is indeed the same dispersion relation as in Eq. (4.10).

4.2.2 Dirac Hamiltonian

Dirac has developed his relativistic description in a four-dimensional space-time. In the case of graphene, we can neglect the third space direction z. Therefore, we are working in further calculations in a three-dimensional space-time, i.e. we have two space directions x and y as well as one time t.
As wee have seen in the previous section 4.2.1, we obtain the same results in the effective description. Referring to Eq. (3.20), we define

$$\mathcal{H}_{\vec{k}} = -t \begin{pmatrix} 0 & \epsilon(\vec{k}) \\ \epsilon^*(\vec{k}) & 0 \end{pmatrix}. \tag{4.27}$$

All the information about the energy is stored in the matrix $\mathcal{H}_{\vec{k}}$ in Eq. (4.27) above. At low-energies we can linearize this matrix around K and K', and obtain a continuum approximation.
Let us start by expanding the factor $\epsilon(\vec{k})$ in Eq. (3.19) around K and K' which are given in

Eq. (2.12). In first order approximation around K we obtain

$$\begin{aligned}\epsilon(K+\Delta\vec{k}) &= \exp\big(i(K+\Delta\vec{k})\cdot(2\vec{e}_A+\vec{a}_1+\vec{a}_2)\big)\\ &\quad\times\Big[1+\exp\big(-i(K+\Delta\vec{k})\cdot\vec{a}_1\big)+\exp\big(-i(K+\Delta\vec{k})\cdot\vec{a}_2\big)\Big]\\ &\approx \exp\big(i(K+\Delta\vec{k})\cdot(2\vec{e}_A+\vec{a}_1+\vec{a}_2)\big)\\ &\quad\times\Big[1+\exp\big(-iK\cdot\vec{a}_1\big)(1-i\vec{a}_1\cdot\Delta\vec{k})+\exp\big(-iK\cdot\vec{a}_2\big)(1-i\vec{a}_2\cdot\Delta\vec{k})\Big].\end{aligned} \tag{4.28}$$

By using the relations

$$K\,\vec{a}_1=\frac{4\pi}{\sqrt{3}\,a}\begin{pmatrix}-\frac{\sqrt{3}}{6}\\ \frac{1}{2}\end{pmatrix}\cdot a\begin{pmatrix}1\\0\end{pmatrix}=-\frac{2\pi}{3}, \tag{4.29}$$

$$K\,\vec{a}_2=\frac{4\pi}{\sqrt{3}\,a}\begin{pmatrix}-\frac{\sqrt{3}}{6}\\ \frac{1}{2}\end{pmatrix}\cdot a\begin{pmatrix}\frac{1}{2}\\ \frac{\sqrt{3}}{2}\end{pmatrix}=\frac{2\pi}{3}, \tag{4.30}$$

$$K\perp\vec{e}_A\Rightarrow K\cdot\vec{e}_A=0, \tag{4.31}$$

we obtain

$$\begin{aligned}\epsilon(K+\Delta\vec{k}) &\approx \exp\big(i\,\Delta\,\vec{k}\cdot(2\vec{e}_A+\vec{a}_1+\vec{a}_2)\big)\\ &\quad\times\underbrace{\big[1+\exp(-i\frac{2\pi}{3})+\exp(i\frac{2\pi}{3})}_{=1+2\,\cos(\frac{2\pi}{3})=0}+\exp(-i\frac{2\pi}{3})\,i\Delta\vec{k}\cdot\vec{a}_1+\exp(i\frac{2\pi}{3})\,i\Delta\vec{k}\cdot\vec{a}_2\big]\\ &= \exp\big(i\,\Delta\,\vec{k}\cdot(2\vec{e}_A+\vec{a}_1+\vec{a}_2)\big)\,(-i\,\Delta\vec{k})\cdot\big[\exp(-i\frac{2\pi}{3})\vec{a}_1+\exp(i\frac{2\pi}{3})\vec{a}_2\big].\end{aligned} \tag{4.32}$$

By considering geometrical symmetries, we are able to eliminate the factor

$$\exp\big(i\,\Delta\,\vec{k}\cdot(2\vec{e}_A+\vec{a}_1+\vec{a}_2)\big), \tag{4.33}$$

in Eq. (4.32) and obtain finally

$$\begin{aligned}\epsilon(K+\Delta\vec{k}) &\approx -i\,\Delta\vec{k}\cdot\big[\exp(-i\frac{2\pi}{3})\vec{a}_1+\exp(i\frac{2\pi}{3})\vec{a}_2\big]\\ &= -i\big[\big(-\frac{1}{2}-\frac{\sqrt{3}}{2}i\big)\,a\,\Delta k_x+\big(-\frac{1}{2}+\frac{\sqrt{3}}{2}i\big)\big(\frac{a}{2}\Delta k_x+\frac{\sqrt{3}\,a}{2}\Delta k_y\big)\big]\\ &= \frac{\sqrt{3}\,a}{2}\big[\big(-\frac{1}{2}-\frac{\sqrt{3}}{2}i\big)\Delta k_x+\big(\frac{\sqrt{3}}{2}-\frac{1}{2}i\big)\Delta k_y\big]\\ &= \frac{\sqrt{3}\,a}{2}\big[\big(-\frac{1}{2}\Delta k_x+\frac{\sqrt{3}}{2}\Delta k_y\big)+\big(-\frac{\sqrt{3}}{2}i\,\Delta k_x-\frac{1}{2}i\,\Delta k_y\big)\big]\\ &= \frac{\sqrt{3}\,a}{2}\begin{pmatrix}1 & i\end{pmatrix}\begin{pmatrix}\cos(\frac{4\pi}{3}) & -\sin(\frac{4\pi}{3})\\ \sin(\frac{4\pi}{3}) & \cos(\frac{4\pi}{3})\end{pmatrix}\begin{pmatrix}\Delta k_x\\ \Delta k_x\end{pmatrix}.\end{aligned} \tag{4.34}$$

With the Laue condition in Eq. (2.8), we have extracted a rotation matrix in Eq. (4.34). Thanks to this, we rotate and stretch the basis $\{k_x,k_y\}$ by an angle $\frac{4\pi}{3}$ and by a scalar $\hbar$ and obtain a new basis p_1,p_2, i.e. we simplify the factor in Eq. (4.34) to

$$\epsilon(\vec{p})=\frac{\sqrt{3}\,a}{2\hbar}(p_x+ip_y). \tag{4.35}$$

Re-using the steps from Eq. (4.28) up to Eq. (4.35), we can rewrite the matrix $\mathcal{H}_{\vec{k}}$ in Eq. (4.27) evaluated in the point $\vec{k} = K$ and obtain the Dirac Hamiltonian $\mathcal{H}_K$ for low-energy, i.e. we get

$$\mathcal{H}_K = -t \begin{pmatrix} 0 & \epsilon(K) \\ \epsilon^*(K) & 0 \end{pmatrix} = \frac{\sqrt{3}\,a\,t}{2\hbar} \begin{pmatrix} 0 & p_x + i p_y \\ p_x - i p_y & 0 \end{pmatrix} = \frac{\sqrt{3}\,a\,t}{2\hbar} \underbrace{\begin{pmatrix} \sigma_1 & \sigma_2 \end{pmatrix}}_{\vec{\alpha}} \begin{pmatrix} p_x \\ p_y \end{pmatrix} = v_F\,\vec{\alpha}\cdot\vec{p}. \tag{4.36}$$

In a similar manner, the Dirac Hamiltonian $\mathcal{H}_{K'}$ is given by

$$\mathcal{H}_{K'} = \frac{\sqrt{3}\,a\,t}{2\hbar} \begin{pmatrix} 0 & p_x - i p_y \\ p_x + i p_y & 0 \end{pmatrix} = \frac{\sqrt{3}\,a\,t}{2\hbar} \underbrace{\begin{pmatrix} \sigma_1 & -\sigma_2 \end{pmatrix}}_{\vec{\alpha}'} \begin{pmatrix} p_x \\ p_y \end{pmatrix} = v_F\,\vec{\alpha}'\cdot\vec{p}. \tag{4.37}$$

In summary, in the framework of an effective low-energy theory we obtain two Hamiltonians which differ in the vector $\vec{\alpha}$, i.e. they are related by $\vec{\alpha}^* = \vec{\alpha}'$. Therefore, we obtain two Dirac Hamiltonians which are given by

$$\mathcal{H}_K = v_F\,\vec{\alpha}\cdot\vec{p}, \tag{4.38}$$

$$\mathcal{H}_{K'} = v_F\,\vec{\alpha}^*\cdot\vec{p}, \tag{4.39}$$

where we use the vector $\vec{\alpha} = (\sigma_1\,,\,\sigma_2)$ consisting of Pauli matrices which are given in Eq. (4.22). In the case of graphene, the second quantity β does not enter the calculation by reason of the massless Dirac fermions.

4.2.3 Solution of the Dirac Equation

The wave function ψ in the Dirac equation consists of two components, i.e. for each Dirac point K and K', we characterize the electron state in the upper component by a quantum mechanical amplitude of finding the electron on sub-lattice A and in the lower component by one of finding the electron on sub-lattice B. In order to solve the Dirac equation, we start therefore with a time-dependent ansatz for electron states at a single Dirac point, which is given by

$$\psi_{\vec{k}}\,(\vec{x},t) = \exp\left[i\left(\vec{k}\cdot\vec{x} - E_{\vec{k}}\,t\right)\right]\,u_{\vec{k}}, \tag{4.40}$$

where we have introduced the eigenvector

$$u_{\vec{k}} = \begin{pmatrix} A \\ B \end{pmatrix}, \tag{4.41}$$

of the energy eigenvalue equation

$$\mathcal{H}_D\,u_{\vec{k}} = E_{\vec{k}}\,u_{\vec{k}}. \tag{4.42}$$

By inserting the ansatz of Eq. (4.40) in Eq. (4.17), evaluated in the Dirac point K, we obtain the eigenvalue

$$E_K^{(\pm)}(\vec{k}) = \pm v_F\,|\vec{k}|, \tag{4.43}$$

and the corresponding eigenvector

$$u_K^{(\pm)} = \pm \begin{pmatrix} 0 & e^{-i\varphi_{\vec{k}}} \\ e^{i\varphi_{\vec{k}}} & 0 \end{pmatrix} u_K^{(\pm)} \quad \Rightarrow \quad u_K^{(\pm)}(\vec{k}) = \frac{1}{\sqrt{2}} \begin{pmatrix} e^{-i\varphi_{\vec{k}}/2} \\ \pm e^{i\varphi_{\vec{k}}/2} \end{pmatrix}, \tag{4.44}$$

where $\varphi_{\vec{k}}$ is the polar angle of the wave vector $\vec{k}$. By evaluating the Dirac equation in the Dirac point K', we obtain self-evidently the same eigenvalue, i.e. $E_K = E_{K'}$. Note that the $\pm$-sign refers to the conduction $(+)$ and valence $(-)$ band, i.e. to electrons in the upper and holes in the lower band. However, eigenvectors in K' differ from eigenvectors in K by the pseudo-spin $\vec{\sigma}$. Therefore, the energy eigenvectors in the Dirac point K' take the form

$$u_{K'}^{(\pm)}(\vec{k}) = \frac{1}{\sqrt{2}} \begin{pmatrix} e^{i\varphi_{\vec{k}}/2} \\ \pm e^{-i\varphi_{\vec{k}}/2} \end{pmatrix}. \tag{4.45}$$

As we see for both Dirac points K and K', the momentum of the massless Dirac fermions is linearly related to their energy. A comparable particle with such a dispersion is the photon which is massless and has a proportional relation between energy and momentum, $E \sim p$, too. In comparison, for massive particles we observe the dispersion relation $E \sim p^2$. Therefore, we obtain in Eq. (4.43) a second evidence for massless Dirac fermions.
By referring to the energy eigenvectors, we introduce a new operator, the helicity h [8], which is given by

$$h = \frac{\vec{\sigma} \cdot \vec{p}}{|\vec{p}|}. \tag{4.46}$$

Obviously, the states ψ_K and $\psi_{K'}$ are also eigenstates of h, i.e. we obtain the eigenvalue equation

$$h\,\psi_{K,K'} = \pm 1\,\psi_{K,K'}, \tag{4.47}$$

where the eigenvalue of h yield $\lambda_h = \pm 1$ for electron states ψ in Dirac point K as well as K'. This property implies that the helicity (or chirality) is well defined around the Dirac points for low-energies. This distinction between electrons (positive helicity) and holes (negative helicity) on each Dirac point becomes important in the following chapter 5.

Chapter 5

Dirac Fermions in a Magnetic Field

In the microscopic model as well as in the effective theory, in previous chapter 4 we found that the Dirac fermions are relativistic, massless particles which move through the lattice with an effective speed of light namely the Fermi velocity $v_f \approx 1 \cdot 10^6 \frac{m}{s}$ [7]. These Dirac fermions in graphene are described by two-component wave functions and have a chiral property for low energies, as we have seen in section 4.2. The symmetry between electrons and holes is an important aspect in the consideration of graphene in an external magnetic field. By applying a constant magnetic field $\vec{B}$ to the 2D honeycomb lattice, we observe a so-called Landau quantization, i.e. the energy spectrum yields discrete energy levels. These generated Landau levels are a crucial ingredient for the explanation of the quantum Hall effect (QHE) which was observed in graphene by applying an additional electrical field $\vec{E}$.
I this last chapter 5, we consider graphene in an external magnetic field, once in the microscopic model of section 3 and once in the effective theory of section 4. In both models, we describe graphene's behavior but only in the effective theory we consider the occurring Landau levels. Finally, we discuss briefly the QHE in graphene in order to show the importance of the Landau quantization.

5.1 Microscopic Model

We extend the Hamiltonian of electron hopping to nearest-neighbors in the presence of a magnetic field by introducing parallel transporters $U_{nm}(\vec{x})$. The applied magnetic field $\vec{B}$ is continuous while the lattice consists of discrete points. Therefore, we define this additional term to describe the influence of the magnetic field on the different types of electron hopping. We define the parallel transporter as

$$U_{nm}(\vec{x}) = \exp\left(i\frac{e}{\hbar}\int_{\vec{x}_n}^{\vec{x}_m} d\vec{x}' \cdot \vec{A}(\vec{x}')\right). \tag{5.1}$$

In other words, the hopping parameter t acquires an additional phase φ_{ij} when we apply a magnetic field to the system, i.e.

$$t = t_{nm}^{(0)} \to t_{nm}^{(B)} = t_{nm}^{(0)} \exp\left(i\varphi_{nm}\right) = t_{nm}^{(0)} \exp\left(i\frac{e}{\hbar}\int_{\vec{x}_n}^{\vec{x}_m} d\vec{x}' \cdot \vec{A}(\vec{x}')\right) = t\, U_{nm}(\vec{x}). \tag{5.2}$$

We consider a constant magnetic field $\vec{B} = B\vec{e}_z$ with corresponding vector potential $\vec{A} = (-yB, 0, 0)$ and apply it to the 2D honeycomb lattice in the x-y plane. To describe the

electron motion in the presence of an external magnetic field, we expand the Hamiltonian in Eq. (3.8) with six different parallel transporters $U_{nm}(\vec{x})$ according to Eq. (5.1). With respect to this, we can rewrite the Hamiltonian in Eq. (3.8) to

$$\begin{aligned}\mathcal{H} = -t \sum_{n_1,n_2,s} \Big[& c^\dagger_{B,s,n_1+1,n_2}\, U_{12}(\vec{x})\, c_{A,s,n_1+1,n_2+1} + c^\dagger_{A,s,n_1+1,n_2}\, U_{23}(\vec{x})\, c_{B,s,n_1+1,n_2} \\ & + c^\dagger_{B,s,n_1,n_2}\, U_{34}(\vec{x})\, c_{A,s,n_1+1,n_2} + c^\dagger_{A,s,n_1,n_2+1}\, U_{45}(\vec{x})\, c_{B,s,n_1,n_2} \\ & + c^\dagger_{B,s,n_1,n_2+1}\, U_{56}(\vec{x})\, c_{A,s,n_1+1,n_2+1} + c^\dagger_{A,s,n_1+1,n_2}\, U_{61}(\vec{x})\, c_{B,s,n_1,n_2+1} \Big], \end{aligned} \tag{5.3}$$

where we simplify the problem by characterizing each lattice site per hexagon by the parameters n_1 and n_2 (see Fig 5.1).

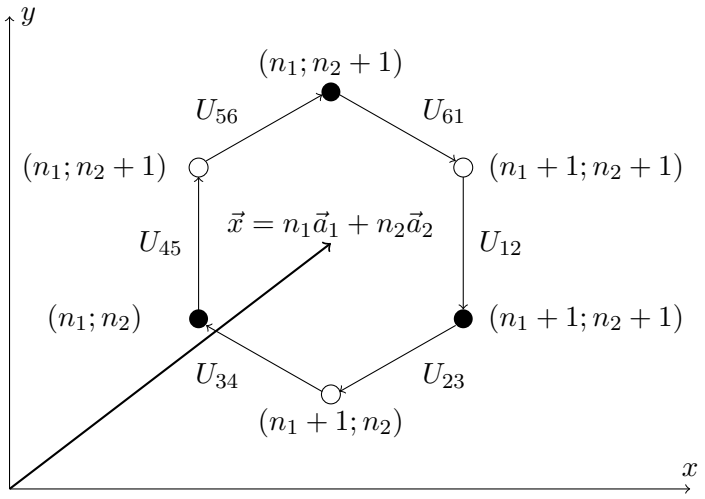

Figure 5.1: Illustration of the six parallel transporters U_{nm} in a single hexagon. The vector $\vec{x}$ points in the middle of a hexagon whereas its parameters n_1 and n_2 characterize the six corners. The arrows from one lattice site to the other indicate the manner of adding the different parallel transporters U_{nm} in the Hamiltonian in Eq. (5.3).

According to appendix B, the six transporters appearing in Eq. (5.3) are given by

$$U_{12}(\vec{x}) = U_{45}(\vec{x}) = 1, \tag{5.4}$$

$$U_{23}(\vec{x}) = U_{34}(\vec{x}) = \exp\left(i\, n_2 \vec{r}\cdot\vec{a}_2 - i\,\phi\right), \tag{5.5}$$

$$U_{56}(\vec{x}) = U_{61}(\vec{x}) = \exp\left(-i\, n_2 \vec{r}\cdot\vec{a}_2 - i\,\phi\right), \tag{5.6}$$

where we have introduced

$$\vec{r} = \left(0\,,\, \frac{e\,B}{2\,\hbar\,c}\,a\right), \quad \phi = \frac{\sqrt{3}\,e\,B}{8\,\hbar\,c}\,a^2. \tag{5.7}$$

To simplify the Hamiltonian in Eq. (5.3), we utilize the shift invariance in x-direction using the vanishing commutation relation $[\mathcal{H}, k_x] = 0$ which we obtain by considering the Landau gauge $\vec{A} = (-yB, 0, 0)$. Thanks to this, we define the Fourier transform of the used creation and annihilation operators similarly to section 3.1, i.e. the Fourier transform is given by

$$\tilde{c}^\dagger_{L,s,n_2}(k_x) = \sum_{n_1} c^\dagger_{L,s,n_1,n_2}\, \exp\left(-i\, k_x\, a\, n_1\right), \tag{5.8}$$

$$\tilde{c}_{L,s,n_2}(k_x) = \sum_{n_1} c_{L,s,n_1,n_2} \, \exp\left(i\, k_x\, a\, n_1\right), \tag{5.9}$$

where we have defined the index $L \in \{A, B\}$, because these definitions are valid for both sub-lattices A and B. The corresponding inverse Fourier transform yields

$$c^{\dagger}_{L,s,n_1,n_2} = \frac{a}{2\,\pi} \int_{-\frac{\pi}{a}}^{\frac{\pi}{a}} dk_x \, \tilde{c}^{\dagger}_{L,s,n_2}(k_x) \exp(-i\, k_x\, a\, n_1), \tag{5.10}$$

$$c_{L,s,n_1,n_2} = \frac{a}{2\,\pi} \int_{-\frac{\pi}{a}}^{\frac{\pi}{a}} dk_x \, \tilde{c}_{L,s,n_2}(k_x) \exp(i\, k_x\, a\, n_1), \tag{5.11}$$

where $k_x \in \left[-\frac{\pi}{a}, \frac{\pi}{a}\right]$ by referring to chapter 2. Finally, we simplify the Hamiltonian in Eq. (5.3) by including the creation and annihilation operators of Eq. (5.10) and Eq. (5.11). In the same manner we have simplified the Hamiltonian in section 3.2.2, we identify a Dirac-δ-function $\delta(k_x - k'_x)$ and obtain a compact form of the Hamiltonian, i.e. we get

$$\begin{aligned}
\mathcal{H} = -t \sum_{n_2,s} \frac{a}{2\pi} \int_{-\frac{\pi}{a}}^{\frac{\pi}{a}} dk \Big[& \tilde{c}^{\dagger}_{B,s,n_2} \, \tilde{c}_{A,s,n_2+1} \\
& + \tilde{c}^{\dagger}_{A,s,n_2+1} \, \tilde{c}_{B,s,n_2} \\
& + \tilde{c}^{\dagger}_{B,s,n_2+1} \, \tilde{c}_{A,s,n_2+1} \, \exp\left(-i\, 2\, \phi\, n_2 - i\, \phi\right) \\
& + \tilde{c}^{\dagger}_{A,s,n_2} \, \tilde{c}_{B,s,n_2} \, \exp\left(i\, 2\, \phi\, n_2 - i\, \phi\right) \\
& + \tilde{c}^{\dagger}_{B,s,n_2} \, \tilde{c}_{A,s,n_2} \, \exp\left(-i\, 2\, \phi\, n_2 - i\, \phi - i\, k_x\, a\right) \\
& + \tilde{c}^{\dagger}_{A,s,n_2+1} \, \tilde{c}_{B,s,n_2+1} \, \exp\left(i\, 2\, \phi\, n_2 - i\, \phi + i\, k_x\, a\right) \Big].
\end{aligned} \tag{5.12}$$

Unlike in section 3.2.3, we are not able to identify the dispersion relation in Eq. (5.12) above. Therefore, we solve the energy eigenvalue equation $\mathcal{H}\,\psi = E\,\psi$ by comparison of coefficients. We then define an electron state ψ as

$$|\psi\rangle = \sum_{n_2,s} \left(a_{A,s,n_2} \, \tilde{c}^{\dagger}_{A,s,n_2} + a_{B,s,n_2} \, \tilde{c}^{\dagger}_{B,s,n_2} \right) |0\rangle, \tag{5.13}$$

where $a_{n_2,L}$ stands for the probability amplitude of sub-lattice $L \in \{A, B\}$, and obtain two iterative recurrence relations of the amplitudes a_{A,s,n_2} and a_{B,s,n_2}, i.e. for $\epsilon := -\frac{E}{t}$ we get

$$\begin{aligned}
\epsilon\, a_{A,s,n_2} &= a_{B,s,n_2-1} + a_{B,s,n_2} \, \exp\left[i\, \phi\, (2n_1 - 1)\right] + a_{B,s,n_2} \, \exp\left[-i\, \phi\, (2n_1 - 1) + i k_x a\right] \\
&= a_{B,s,n_2-1} + a_{B,s,n_2} \, \exp\left(i k_x a\right) \, \cos\left(\phi\, (2n_1 - 1) - \frac{k_x}{2} a\right) \\
&= a_{B,s,n_2-1} + g\, h(n_2)\, a_{B,s,n_2},
\end{aligned} \tag{5.14}$$

$$\begin{aligned}
\epsilon\, a_{B,s,n_2} &= a_{A,s,n_2+1} + a_{A,s,n_2} \, \exp\left[-i\, \phi\, (2n_1 - 1)\right] + a_{A,s,n_2} \, \exp\left[i\, \phi\, (2n_1 - 1) + i k_x a\right] \\
&= a_{A,s,n_2+1} + a_{A,s,n_2} \, \exp\left(-i k_x a\right) \, \cos\left(\phi\, (2n_1 - 1) - \frac{k_x}{2} a\right) \\
&= a_{A,s,n_2+1} + g^{*}\, h(n_2)\, a_{A,s,n_2},
\end{aligned} \tag{5.15}$$

where we have introduced

$$g = \exp(ik_x a), \quad h(n_2) = \cos\left(\phi\,(2n_1 - 1) - \frac{k_x}{2}a\right). \tag{5.16}$$

The thus obtained recursive relations for a_{A,s,n_2} and a_{B,s,n_2} in Eq. (5.14) and (5.15) offer various clues to a relation between both Dirac points K and K' and sub-lattice A and B respectively by applying a magnetic field. A very special aspect arises when we consider the case $E = 0$, i.e. the recursive relations above yield

$$a_{A,s,n_2+1} = -g^*\, h(n_2)\, a_{A,s,n_2}, \tag{5.17}$$

$$a_{B,s,n_2+1} = -\frac{1}{g\, h(n_2)}\, a_{A,s,n_2}, \tag{5.18}$$

which indicates a breaking of the mentioned relation between K and K'. Instead of two recursive relations between amplitudes of both sub-lattices in Eq. (5.14) and (5.15), we obtain two independent relations in Eq. (5.17) and (5.18). In other words, we observe at the zero-energy level, the zeroth Landau level, a doubly-degenerate energy state which is very unusual in the case of conventional semiconductors. In order to be able to analyze the mentioned Landau levels in more detail, we consider the whole problem in an effective description in the following section 5.2. We do not consider Landau levels in the microscopic model, because we have obtained recursive relations as the only description of the dispersion in graphene with applied magnetic field.

5.2 Effective Description

In the case of applying a magnetic field to graphene in the effective description of chapter 4, we start directly from the Dirac Hamiltonians in Eq. (4.38) and (4.39) and solve their eigenvalue equations. Like in the previous section 5.1, we consider the same constant magnetic field $\vec{B} = B\vec{e}_z$ with corresponding vector potential $\vec{A} = (-yB, 0, 0)$ and apply it to the 2D honeycomb lattice in the x-y plane. As we have seen in section 4.2.3, for low energies the electron energy eigenstate ψ is a superposition of two two-component states ψ_K and $\psi_{K'}$. Therefore, in the case of graphene we consider four-component wave functions

$$\psi = \begin{pmatrix} \psi_K \\ \psi_{K'} \end{pmatrix} = \begin{pmatrix} \phi_K^A \\ \phi_K^B \\ \phi_{K'}^A \\ \phi_{K'}^B \end{pmatrix}, \tag{5.19}$$

on which we act with the 4×4 dimensional Hamiltonian

$$\mathcal{H} = v_F \begin{pmatrix} \mathcal{H}_K & 0 \\ 0 & \mathcal{H}_{K'} \end{pmatrix} = v_F \begin{pmatrix} 0 & p_x + ip_y & 0 & 0 \\ p_x - ip_y & 0 & 0 & 0 \\ 0 & 0 & 0 & p_x - ip_y \\ 0 & 0 & p_x + ip_y & 0 \end{pmatrix}. \tag{5.20}$$

5.2.1 Extended Dirac Hamiltonian and Solution

We start by characterizing the application of an external magnetic field $\vec{B}$ to graphene and introduce the $\vec{B}$-field through a minimal coupling which is given by

$$\vec{p} \to \vec{p} + \frac{e\,\vec{A}}{c} = -i\hbar\vec{\nabla} - \frac{e\,B}{c}\,y\,\vec{e}_x, \tag{5.21}$$

where e denotes the positive electron charge. We apply this extended momentum of Eq. (5.21) in Eq. (5.20) and obtain

$$\mathcal{H} = \begin{pmatrix} 0 & \frac{\hbar}{i}\partial_x + \hbar\partial_y - \frac{e\,B}{c}y & 0 & 0 \\ \frac{\hbar}{i}\partial_x - \hbar\partial_y - \frac{e\,B}{c}y & 0 & 0 & 0 \\ 0 & 0 & 0 & \frac{\hbar}{i}\partial_x - \hbar\partial_y - \frac{e\,B}{c}y \\ 0 & 0 & \frac{\hbar}{i}\partial_x + \hbar\partial_y - \frac{e\,B}{c}y & 0 \end{pmatrix}. \tag{5.22}$$

Due to the decoupling of Dirac Hamiltonian $\mathcal{H}_K$ and $\mathcal{H}_{K'}$, we first look for solutions of the eigenvalue equation $\mathcal{H}_K\,\psi = E\,\psi$. Using this, we start with the ansatz

$$\psi_k^K(x,y) = \exp(i\,k\,x)\begin{pmatrix} c_1\,\phi_1^A(y) \\ c_2\,\phi_2^B(y) \end{pmatrix}, \tag{5.23}$$

which is labeled by two indices, namely the Dirac point K and the wave vector component k along the x-axis. The parameters c_1 and c_2 stand for the probability amplitude ϕ_1^A and ϕ_2^B. By inserting this ansatz in the eigenvalue equation of $\mathcal{H}_K$, we obtain

$$v_F\begin{pmatrix} 0 & \frac{\hbar}{i}ik + \hbar\partial_y - \frac{e\,B}{c}y \\ \frac{\hbar}{i}ik - \hbar\partial_y - \frac{e\,B}{c}y & 0 \end{pmatrix}\begin{pmatrix} c_1\phi_1^A \\ c_2\phi_2^B \end{pmatrix} = E\begin{pmatrix} c_1\phi_1^A \\ c_2\phi_2^B \end{pmatrix}. \tag{5.24}$$

Like the conventional Landau quantization in a 2D electron gas (see section 5.2.2), we introduce the so-called *magnetic length* $l_B = \sqrt{\frac{c\hbar}{e\,B}}$ [17] in order to simplify the expression in Eq. (5.24), i.e. we obtain

$$\frac{v_F\hbar}{l_B}\begin{pmatrix} 0 & l_Bk + l_B\partial_y - \frac{y}{l_B} \\ l_Bk - l_B\partial_y - \frac{y}{l_B} & 0 \end{pmatrix}\begin{pmatrix} c_1\phi_1^A \\ c_2\phi_2^B \end{pmatrix} = E\begin{pmatrix} c_1\phi_1^A \\ c_2\phi_2^B \end{pmatrix}. \tag{5.25}$$

In a second step, we rewrite the eigenvalue equation above in components and get two combined relations which are given by

$$\frac{v_F\hbar}{l_B}(\tilde{y} + \partial_{\tilde{y}})\,c_2\phi_2^B = Ec_1\phi_1^A, \tag{5.26}$$

$$\frac{v_F\hbar}{l_B}(\tilde{y} - \partial_{\tilde{y}})\,c_1\phi_1^A = Ec_2\phi_2^B, \tag{5.27}$$

where we have used the substitutions $\tilde{y} = l_Bk - \frac{y}{l_b}$ and $\partial_{\tilde{y}} = l_B\partial_y$ for further simplifications. Finally, we insert Eq. (5.27) in (5.26) and get

$$\left(\frac{v_F\hbar}{l_B}\right)^2(\tilde{y} + \partial_{\tilde{y}})(\tilde{y} - \partial_{\tilde{y}})\,c_1\phi_1^A = E^2c_1\phi_1^A, \tag{5.28}$$

An interesting aspect of this Eq. (5.28) is its form analogous to an eigenvalue equation of a one-dimensional harmonic oscillator in quantum mechanics. By referring to appendix C, we define an annihilation operator a and a creation operator $a^\dagger$ by

$$a = \frac{1}{\sqrt{2}} \left(\tilde{y} + \partial_{\tilde{y}} \right), \tag{5.29}$$

$$a^\dagger = \frac{1}{\sqrt{2}} \left(\tilde{y} - \partial_{\tilde{y}} \right), \tag{5.30}$$

and insert them in Eq. (5.28). After all, for the Dirac point K we obtain an eigenvalue equation which can be solved by defining the wave functions $\phi_n(\tilde{y})$ as solutions of a harmonic oscillator with energy levels n, i.e. with $\phi_1^A \to \phi_{n-1}^A$ we get

$$\left(\sqrt{2} \frac{v_F \hbar}{l_B} \right)^2 a a^\dagger c_{n-1} \phi_{n-1}^A = E^2 c_{n-1} \phi_{n-1}^A, \tag{5.31}$$

and obtain

$$\left(\sqrt{2} \frac{v_F \hbar}{l_B} \right)^2 a a^\dagger c_{n-1} \phi_{n-1}^A = \underbrace{\left(\sqrt{2} \frac{v_F \hbar}{l_B} \right)^2 \sqrt{n} \sqrt{n}}_{=: E_K^2} c_{n-1} \phi_{n-1}^A, \tag{5.32}$$

where we have used the harmonic oscillator relations in Eq. (C.5). By considering the eigenvalue equation of $\mathcal{H}_K$ once more with the eigenvalue E_K obtained above, we get the corresponding eigenvectors as

$$\begin{pmatrix} c_1 \phi_1^A(y) \\ c_2 \phi_2^B(y) \end{pmatrix} = \begin{pmatrix} \phi_{n-1}^A(\tilde{y}) \\ \pm \phi_n^B(\tilde{y}) \end{pmatrix}, \tag{5.33}$$

and solve the problem. In the case of Dirac point K', we simply repeat the steps above with $\phi_2^B \to \phi_n^B$ and develop the solution in a very similar way.
By summarizing the whole extension of the Dirac Hamiltonian in Eq. (5.20) for an applied external magnetic field $\vec{B}$, we obtain a doubly-degenerate energy eigenvalue equal for both Dirac points K and K' which is given by

$$E_n = E_n^K = E_n^{K'} = \pm v_F \sqrt{\frac{2\hbar e B}{c} n} = \pm \hbar \omega_D \sqrt{n}, \quad n \in \mathbb{N}_0, \tag{5.34}$$

where we have introduced $\omega_D = v_F \sqrt{\frac{2eB}{\hbar c}}$ which we interpret as the cyclotron frequency for Dirac fermions (see previous section 5.2.2). The corresponding eigenvectors are given by

$$\psi_{n,k}^K = C_n \exp\left(i k_x x \right) \begin{pmatrix} \phi_{n-1}^A(\tilde{y}) \\ \pm \phi_n^B(\tilde{y}) \\ 0 \\ 0 \end{pmatrix}, \tag{5.35}$$

for Dirac point K and by

$$\psi_{n,k}^{K'} = C_n \exp\left(i k_x x \right) \begin{pmatrix} 0 \\ 0 \\ \phi_n^A(\tilde{y}) \\ \pm \phi_{n-1}^B(\tilde{y}) \end{pmatrix}, \tag{5.36}$$

for Dirac point K'. These eigenvectors are labeled with a third index n which indicates the current Landau level of the electron state. By referring to the double-degeneracy of the eigenvalue, we normalize the eigenvectors $\psi^K_{n,k}$ and $\psi^{K'}_{n,k}$ with an additional constant parameter C_n which is given by

$$C_n = \begin{cases} 1 & n = 0 \\ \frac{1}{\sqrt{2}} & n \neq 0 \end{cases}. \tag{5.37}$$

The wave functions ϕ^L_n for $L \in \{A, B\}$ in Eq. (5.35) and (5.36) are eigenvectors of a one-dimensional harmonic oscillator, oscillating around $l_B\, k$. By referring to Eq. (C.7), we obtain

$$\phi^L_n(x) \propto \exp\left(-\frac{\tilde{y}}{2}\right) H_n(\tilde{y}) = \exp\left(-\frac{1}{2}\frac{(l_B^2 k - y)^2}{l_B^2}\right) H_n\left(\frac{(l_B^2 k - y)}{l_B}\right), \tag{5.38}$$

where the Hermite polynomials are given in Eq. (C.8).
We finish this section by considering the zero-energy level E_0 in more detail. In Eq. (5.34) for all $n > 0$ we observe two equal energy values with opposite sign, i.e. we obtain the energy for electrons (positive sign) and for holes (negative sign) in both Dirac points K and K' respectively. In the case of $n = 0$, the energy is equal to zero for electrons as well as for holes and we obtain the zero points of the dispersion relation. By considering the eigenvectors for $n = 0$, we obtain

$$\psi^K_{0,k} = C_n \exp(ik_x x) \begin{pmatrix} 0 \\ \phi^B_0(\tilde{y}) \\ 0 \\ 0 \end{pmatrix}, \quad \psi^{K'}_{0,k} = C_n \exp(ik_x x) \begin{pmatrix} 0 \\ 0 \\ \phi^A_0(\tilde{y}) \\ 0 \end{pmatrix}. \tag{5.39}$$

Given the helicity at the end of section 4.2.3, the ground state is filled by electrons and holes in equal parts, i.e. we obtain at $E_0 = 0$ two linearly independent electron states as we see in Eq. (5.39). In the following section 5.2.2, we use this interesting aspect of graphene as an essential observation in the consideration of the quantum Hall effect (QHE).

5.2.2 Landau Levels and Anomalous Quantum Hall Effect

By applying an external magnetic field perpendicular to the graphene sheet, the energy spectrum becomes discrete, as we have seen in the previous section 5.2.1. In comparison with Landau quantization in a 2D electron gas or 2D semiconductor, graphene represents a special case. Therefore, we first briefly discuss the conventional Landau quantization, such that we are able to compare it with the quantization in graphene. Corresponding to these Landau levels, we consider in a second step the three types of Hall effect which we use to finally understand a certain anomaly of the QHE in graphene.
In the case of conventional Landau quantization, the interacting electrons are massive and non-relativistic, we call them Schrödinger fermions. With respect to this, we consider a semiconductor which has nearly a similar dispersion relation to graphene, i.e. it consists of two energy bands touching each other at zero energy. The Landau quantization then leads to discrete and equally spaced energy levels where the first Landau level is observable at a non-zero energy, i.e. the energy eigenvalue takes the form

$$E_n = \pm\hbar\,\omega_c(n + \frac{1}{2}), \quad n \in \mathbb{N}, \tag{5.40}$$

where $\omega_c = \frac{eB}{mc}$ is the so-called cyclotron frequency [18] and the introduced $\pm$-sign refers to the two mentioned energy bands. We call ω_c a cyclotron frequency, because the electrons describe a spiral path along the z-axis while moving through the external magnetic field $\vec{B} = B\,\vec{e}_z$. By considering Dirac fermions again, the energy levels in Eq. (5.34) differ from the energy levels in Eq. (5.40). In fact, Landau levels for Dirac electrons are different from Landau levels for Schrödinger electrons (Fig. 5.2). This enormous difference in the dispersion relation has consequences with respect to the QHE which we discuss next.

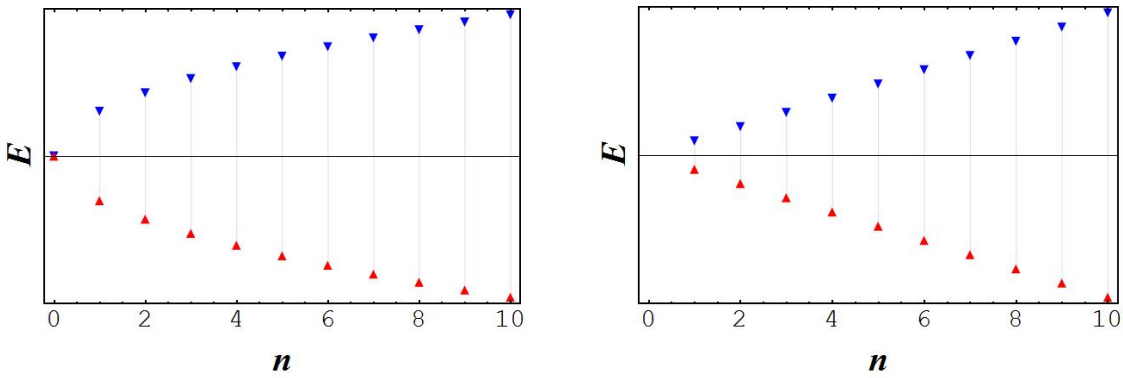

Figure 5.2: Landau levels $n \in [0, 10]$ are illustrated for graphene on the left and for a conventional two band semiconductor on the right. Left: $E_0 = 0$ and $E_n \propto \sqrt{n} \Rightarrow \Delta E \neq const.$ Right: $E_0 \neq 0$ and $E_n \propto n \Rightarrow \Delta E = const.$

In the case of Hall effects, we differentiate between the classical Hall effect and the quantum Hall effect (QHE). Furthermore, we differentiate with regard to the QHE between the integer quantum Hall effect (IQHE) and the fractional quantum Hall effect (FQHE). Obviously, the classical Hall effect was discovered first in 1879 by E. Hall. He discovered a voltage difference, the so-called Hall voltage, across an electrical conductor which was traversed by an electric current in a magnetic field perpendicular to it. The explanation of this effect is quite simple: Given the Lorentz force $\vec{F}$, generated by the electric current with density $\vec{j}$ and the magnetic field $\vec{B} = B\,\vec{e}_z$, the flowing electrons get pushed to one edge of the sample and generate a resulting electric field $\vec{E}$.
To understand the link between the classical and the quantum Hall effect and the remarkable property of graphene in regard to the QHE, we introduce a few definitions (c.f. [18]). We start with the resistivity tensor ρ which is given by

$$\rho = \frac{B}{n\,e\,c} \begin{pmatrix} 0 & 1 \\ -1 & 0 \end{pmatrix}, \tag{5.41}$$

as well as the conductivity tensor σ which takes the form

$$\sigma = \frac{n\,e\,c}{B} \begin{pmatrix} 0 & -1 \\ 1 & 0 \end{pmatrix}, \tag{5.42}$$

where n is the electron density and e the elementary charge. Obviously, the conductivity tensor σ is just the inverse of the resistivity tensor ρ. Therefore, they are both connected to the resulting electric field $\vec{E}$, i.e. we get

$$\vec{E} = \rho\,\vec{j}, \quad \vec{j} = \sigma\,\vec{E}. \tag{5.43}$$

Finally, we define the x-y component of the resistivity tensor ρ in Eq. (5.41) as the Hall resistivity which is given by

$$R_H := \rho_{xy} = \frac{B}{n\,e\,c} = \frac{U_H}{I}, \tag{5.44}$$

and the y-x component of the conductivity tensor σ in Eq. (5.42) as the Hall conductivity, i.e. we obtain

$$\sigma_{yx} = \frac{n\,e\,c}{B}. \tag{5.45}$$

In the case of the classical Hall effect, in Eq. (5.44) we obtain a linear relation between the magnetic field $\vec{B}$ and the electron density n. Therefore, we are able to determine, for example, with this effect electron densities by known magnetic field or vice versa.
By switching from the classical Hall effect to the QHE, the basic experimental set-up remains nearly the same. The effect is exclusively observable in two-dimensional metals such as bounding surfaces on which we are able to describe the electrons as a 2D electron gas and this only at sufficiently low temperature. When we drastically reduce the temperature of a sample, the Hall resistivity becomes independent of the magnetic field and forms a quantized Hall plateau. Therefore, the relation in Eq. (5.44) becomes incorrect and we obtain in the case of the QHE a Hall resistivity which is given by

$$\rho_{xy} = \frac{h}{\nu\,e^2}, \tag{5.46}$$

where ν is an integer and h is Planck's quantum [18]. Similarly, we rewrite the Hall conductivity which takes the form

$$\sigma_{yx} = \frac{e^2}{h}\nu. \tag{5.47}$$

K. von Klitzing was first to discover the IQHE explained above in 1980. Only two years later in 1982, D. Tsui, H. Störmer and A. Gossard discovered the FQHE. In both types, the Hall conductivity is given by Eq. (5.47), but the Hall plateaux appear at different values of ν, i.e. in the case of the IQHE the parameter ν is an integer number while in the case of the FQHE the parameter ν is a fractional number (e.g. $\nu = \frac{1}{3}$ or $\nu = \frac{2}{5}$).
By using the explanations of the QHE above in the case of graphene, we obtain finally an anomalous quantum Hall Effect (AQHE), i.e. a fourth type which differs from the others. By referring to section 5.2.1, the first Landau level is observable at zero energy. For this reason, the first Hall plateau then appears already when the lowest Landau level is half-filled, i.e. the Hall conductivity takes the form

$$\sigma_{yx} = \pm 4\frac{e^2}{h}(i + \frac{1}{2}), \quad i \in \mathbb{N}, \tag{5.48}$$

by referring to [7]. The factor 4 in Eq. (5.48) is introduced through the degeneracy which we have discussed at the beginning of section 5.2 and the $\pm$-sign refers to the electrons in the conduction band $(+)$ and to the holes in the valence band $(-)$.
The very interesting aspect about this AQHE is not only the different Hall plateaux in comparison with IQHE and FQHE but also the temperature at which we observe the QHE in graphene. Due to the large cyclotron gap $\hbar\omega_D$ in Eq. (5.34) between the zeroth and the first Landau level (Fig. 5.2), the QHE in graphene is even observable at room temperature [19] and makes graphene an essential tool for verifying basic knowledge in quantum mechanics. In addition, this AQHE is the most direct evidence for Dirac fermions.

Obviously, there is an enormous number of interesting topics which are concerning the AQHE in graphene. Unfortunately, we would extend this Bachelor thesis too much by considering the whole theory in detail. Therefore, this last section is presented as a introduction to an important application of the Landau quantization, i.e. it should motivate further research in this area.

Chapter 6

Conclusion

At the beginning of my thesis in chapter 2, we became acquainted with graphene as a stable 2D non-Bravais lattice which consists of two Bravais sub-lattices A and B. We described graphene's hexagonal structure with basic tools of solid-state physics and prepared the Fourier transform for computations in further chapters. In chapter 3, we started developing the first Hamiltonian based on the single-band Hubbard model (electron hopping to nearest-neighbors). After diagonalizing it, we extracted the dispersion relation and obtained two symmetric energy bands namely the upper conduction and lower valence band. In a second step, the interacting electrons were allowed to hop to nearest- and next-to-nearest-neighbor ions as well and we extended the energy operator. It turned out that the allowing of hopping to next-to-nearest-neighbors yields a certain electron-hole asymmetry. By going forward, we repeated in chapter 4 the description of electron motion but this time in an effective theory at low energy. By approximating the energy around the Dirac points K and K', we obtained a linear characteristic, the defined Dirac cones. Such a behavior is comparable with massless photons which have a linear dispersion relation, too. Therefore, we obtained first evidence of massless fermions in graphene. In a second step, we developed an effective Hamiltonian based on the Dirac equation which we solved for low energies. We obtained finally as a result of the whole chapter 4, that the interacting electrons in graphene are in fact describable as relativistic, massless Dirac fermions. Finally in chapter 5, we extended the microscopical model as well as the effective description in the case of a magnetic field. The consequence of an applied magnetic field perpendicular to graphene is the quantization of the energy spectrum into discrete Landau levels. We observed an enormous difference between the Landau quantization in conventional semiconductors and graphene which yields an observable anomalous quantum Hall effect (AQHE) when we apply an additional electric field along the lattice. Even at room temperature, we witnessed a quantum Hall effect which forms Hall plateaux at half-integer values. The existence of the AQHE is the most direct evidence of Dirac fermions in graphene.

In many respects, graphene is a remarkable, unique system. It differs in many ways from conventional metals as well as semiconductors and brings a lot of important fundamental physics aspects with it. Therefore, I attempted in my thesis to emphasize in particular the peculiarities of graphene by using basic knowledge on the level of undergraduate students. To finish my work, I give in the following section 6.1 a brief outlook and explain one possible application of graphene in detail.

6.1 Outlook

The research concerning graphene is in full activity, because this new material is promising a lot of application possibility. For example, graphene could exchange mono-crystalline silicon layer in solar cells or be a building material for ballistic transistors by referring to their high electronic quality. With respect to its additional high optical transparency, graphene is a candidate in developing touch-screens.
A very interesting application of graphene are electronic devices at nano-scale. A team of researchers from Berkeley works on a possibility to control electron motions in graphene such that they can produce for example a digital signal, i.e. an electron current which they could turn on or off. As we saw already in chapter 3, graphene is a zero-gap semiconductor, i.e. one has to produce an artificial band gap for graphene to behave like a conventional semiconductor. Wang et al. [20] found a method to control this current by considering a bilayer of graphene (Fig. 6.1). In an external electric field two stacked layer of graphene produce in fact a band gap which breaks the electron current in graphene until it gets switched off again. With this method, we are able to optimize devices of semiconductors or build up new kinds of transistors at nano-scale.

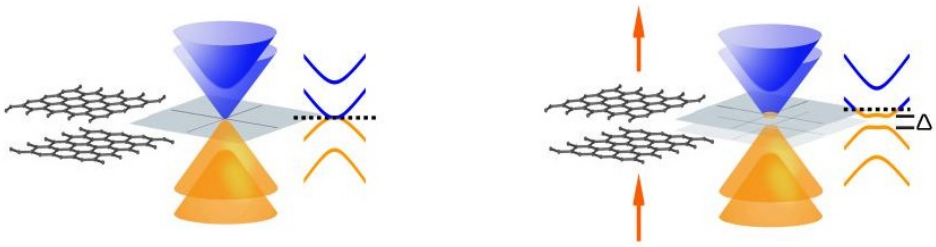

Figure 6.1: Schematic demonstration of bilayer graphene (left) in an external electric field (right). The electric field (arrows) separate the conduction band (blue) from the valence band (yellow) which are connected at the Fermi level (dotted line) and generates a band gap (Δ) [20].

To cut a long story short, graphene could revolutionize as a new material a number of different fields. Therefore, it is justified to say: A promising future is only a pencil away.

Appendix A

Kronecker-Delta and Delta-Function

To derive the Kronecker-δ of Eq. (2.23), we start with the inverse Fourier Transform

$$f_{\vec{x}} = \int_{-\frac{1}{2}}^{\frac{1}{2}} dm_1 \int_{-\frac{1}{2}}^{\frac{1}{2}} dm_2 \, \tilde{f}(\vec{k}) \exp(i\vec{k}\cdot\vec{x}) = \frac{\sqrt{3}\,a^2}{8\pi^2} \int_B d^2k \, \tilde{f}(\vec{k}) \, \exp(i\vec{k}\cdot\vec{x}) \tag{A.1}$$

The Fourier Transform of a Kronecker-δ is equal to 1, so we get for all $\vec{x} \neq \vec{0}$

$$\int_{-\frac{1}{2}}^{\frac{1}{2}} dm_1 \int_{-\frac{1}{2}}^{\frac{1}{2}} dm_2 \, \exp(i\vec{k}\cdot\vec{x}) = \int_{-\frac{1}{2}}^{\frac{1}{2}} dm_1 \int_{-\frac{1}{2}}^{\frac{1}{2}} dm_2 \, \exp\left[2\pi i(m_1 n_1 + m_2 n_2)\right]$$

$$= -\frac{1}{4\pi n_1 n_2}\big[\exp(\pi i n_1) - \exp(-\pi i n_1) + \exp(\pi i n_2) - \exp(-\pi i n_2)\big] = 0 \quad \forall n_{1,2} \in \mathbb{Z} \tag{A.2}$$

For $\vec{x} = \vec{0}$ we get

$$\int_{-\frac{1}{2}}^{\frac{1}{2}} dm_1 \int_{-\frac{1}{2}}^{\frac{1}{2}} dm_2 \, \exp(i\vec{k}\cdot\vec{0}) = \int_{-\frac{1}{2}}^{\frac{1}{2}} dm_1 \int_{-\frac{1}{2}}^{\frac{1}{2}} dm_2 = 1 \tag{A.3}$$

Using Eq. (A.2) and Eq. (A.3) we can write a Kronecker-Delta, which is given by

$$\delta_{\vec{x},0} = \frac{\sqrt{3}\,a^2}{8\pi^2} \int_B d^2k \, \exp(i\vec{k}\cdot\vec{x}), \tag{A.4}$$

where the inverse function takes form to

$$\delta(\vec{k}) = \frac{\sqrt{3}\,a^2}{8\pi^2} \sum_{\vec{x}} \exp(-i\vec{k}\cdot\vec{x}) \tag{A.5}$$

Appendix B

Parallel Transporter

According to the definition in Eq. (5.1), the six transporters appearing in Eq. (5.3) are given by

$$U_{12}(\vec{x}) = \exp\left(i\frac{e}{\hbar}\int_{\vec{x}+\vec{e}_A}^{\vec{x}+\vec{e}_B+\vec{a}_1} d\vec{x}'\cdot\vec{A}(\vec{x}')\right) = 1, \tag{B.1}$$

$$U_{23}(\vec{x}) = \exp\left(i\frac{e}{\hbar}\int_{\vec{x}+\vec{e}_B+\vec{a}_1}^{\vec{x}+\vec{e}_A-\vec{a}_2} d\vec{x}'\cdot\vec{A}(\vec{x}')\right) = \exp\left[i\frac{e\,B}{\hbar}\left(-\frac{\sqrt{3}}{8}a^2+\frac{x_2}{2}a\right)\right], \tag{B.2}$$

$$U_{34}(\vec{x}) = \exp\left(i\frac{e}{\hbar}\int_{\vec{x}+\vec{e}_A-\vec{a}_2}^{\vec{x}+\vec{e}_B} d\vec{x}'\cdot\vec{A}(\vec{x}')\right) = \exp\left[i\frac{e\,B}{\hbar}\left(-\frac{\sqrt{3}}{8}a^2+\frac{x_2}{2}a\right)\right], \tag{B.3}$$

$$U_{45}(\vec{x}) = \exp\left(i\frac{e}{\hbar}\int_{\vec{x}+\vec{e}_B}^{\vec{x}+\vec{e}_A-\vec{a}_1} d\vec{x}'\cdot\vec{A}(\vec{x}')\right) = 1, \tag{B.4}$$

$$U_{56}(\vec{x}) = \exp\left(i\frac{e}{\hbar}\int_{\vec{x}+\vec{e}_A-\vec{a}_1}^{\vec{x}+\vec{e}_B+\vec{a}_2} d\vec{x}'\cdot\vec{A}(\vec{x}')\right) = \exp\left[i\frac{e\,B}{\hbar}\left(-\frac{\sqrt{3}}{8}a^2-\frac{x_2}{2}a\right)\right], \tag{B.5}$$

$$U_{61}(\vec{x}) = \exp\left(i\frac{e}{\hbar}\int_{\vec{x}+\vec{e}_B+\vec{a}_2}^{\vec{x}+\vec{e}_A} d\vec{x}'\cdot\vec{A}(\vec{x}')\right) = \exp\left[i\frac{e\,B}{\hbar}\left(-\frac{\sqrt{3}}{8}a^2-\frac{x_2}{2}a\right)\right]. \tag{B.6}$$

To simplify the obtained U_{nm}, we define two new constant parameters. With Eq. (5.7), the parallel transporters finally take the form

$$U_{12}(\vec{x}) = U_{45}(\vec{x}) = 1, \tag{B.7}$$

$$U_{23}(\vec{x}) = U_{34}(\vec{x}) = \exp\left(i\,\vec{r}\cdot\vec{x} - i\,\phi\right) = \exp\left(i\,n_2\vec{r}\cdot\vec{a}_2 - i\,\phi\right), \tag{B.8}$$

$$U_{56}(\vec{x}) = U_{61}(\vec{x}) = \exp\left(-i\,\vec{r}\cdot\vec{x} - i\,\phi\right) = \exp\left(-i\,n_2\vec{r}\cdot\vec{a}_2 - i\,\phi\right), \tag{B.9}$$

where we have used $\vec{x} = n_1\vec{a}_1 + n_2\vec{a}_2$.

Appendix C

Quantum Harmonic Oscillator

In Eq. (5.28) we observe a certain analogy to the eigenvalue equation of a harmonic oscillator in quantum mechanics. To verify this assumption, we resume quickly some basic knowledge by starting with the energy eigenvalue equation of a one-dimensional harmonic oscillator which is given by

$$\mathcal{H}\,\phi(z) = \left[-\frac{\hbar^2}{2m}\partial_z^2 + \frac{1}{2}m\omega^2 z^2\right]\phi(z) = E\phi(z). \tag{C.1}$$

By defining annihilation and creation operators as

$$a = \sqrt{\frac{m\omega}{2\hbar}}\left(z + \frac{\hbar}{m\omega}\partial_z\right), \quad a^\dagger = \sqrt{\frac{m\omega}{2\hbar}}\left(z - \frac{\hbar}{m\omega}\partial_z\right), \tag{C.2}$$

Eq. (C.1) leads to

$$\mathcal{H}\,\phi(z) = \hbar\omega\left(\mathcal{N} + \frac{1}{2}\right)\phi(z), \tag{C.3}$$

where the number operator is defined as $\mathcal{N} = a^\dagger a$. This operator has the eigenvalues $n = 0, 1, 2, 3, ...$ and the eigenvectors

$$\phi_0 = \left(\frac{\hbar}{\pi m\omega}\right)^{1/4}, \quad \phi_n = \frac{1}{\sqrt{n!}}\left(a^\dagger\right)^n\phi_0. \tag{C.4}$$

By considering a single annihilation or creation operator, respectively, which act on a wave function, we obtain the following rules:

$$a\phi_n = \sqrt{n}\phi_{n-1}, \quad a^\dagger\phi_n = \sqrt{n+1}\phi_{n+1}, \quad a\phi_0 = 0. \tag{C.5}$$

Finally, the eigenvalue in Eq. (C.3) reads

$$E_n = \hbar\,\omega\left(n + \frac{1}{2}\right), \tag{C.6}$$

and the corresponding eigenvectors in Eq. (C.4) lead to

$$\phi_n(x) = \sqrt{\frac{1}{2^n\,n!}}\left(\frac{m\,\omega}{\pi\hbar}\right)^{1/4}\exp\left(-\frac{m\omega x^2}{2\hbar}\right)\,H_n\left(\sqrt{\frac{m\omega}{\hbar}}\,x\right), \tag{C.7}$$

where the functions H_n, the so called Hermite polynomials, are given by

$$H_n(x) = (-1)^n\exp\left(x^2\right)\frac{d^n}{dx^n}\left(\exp\left(-x^2\right)\right). \tag{C.8}$$

Bibliography

[1] H. H. Binder, *Lexikon der chemischen Elemente*, S. Hirzel Verlag, (1999).

[2] B. C. Brodie, *On the Atomic Weight of Graphite*, Proceedings of the Royal Society of London, (1859).

[3] H. P. Boehm, R. Setton, E. Stumpp, *Nomenclature and terminology of graphite intercalation compounds*, Pure and Applied Chemistry, (1994).

[4] The Nobel Prize in Physics 2010, `http://nobelprize.org/nobel_prizes/physics/laureates/2010/` (08.06.2011).

[5] N. D. Mermin, Phys. Rev. 176, 250, (1968).

[6] V. Geringer, M. Liebmann, T. Echtermeyer, S. Runte, M. Schmidt, R. Rückamp, M. Lemme, M. Morgenstern, arXiv:0806.1028v3 [cond-mat.mtrl-sci](2008).

[7] A. H. Castro Neto, F. Guinea, N. M. R. Peres, K. S. Novoselov and A. K. Geim, arXiv:0709.1163v2 [cond-mat.other](2008).

[8] J. Balmer, lecture notes: *Festkörperphysik*, Universität Bern, (2010).

[9] N. W. Ashcroft, N. D. Mermin, Solid State Physics, Holt, Rinehart and Winston, (1976).

[10] U.-J. Wiese, lecture notes: *Statistical Mechanics*, Universität Bern, (2010).

[11] P. R. Wallace, Phys. Rev. 71, 622, (1947).

[12] R. S. Deacon, K.-C. Chuang, R. J. Nicholas, K. S. Novoselov, and A. K. Geim, Phys. Rev. B 76, 081406, (2007).

[13] S. Reich, J. Maultzsch, and C. Thomsen, Phys. Rev. B 66, 035412, (2002).

[14] A. Rubbia, lecture notes: *Teilchenphysik*, ETH Zürich, (2002).

[15] M. I. Katsnelson, K. S. Novoselov and A. K. Geim, Nat. Phys. 2, 620 - 625, (2006).

[16] P. Hasenfratz, lecture notes: *Quantentheorie*, Universität Bern, (2009 / 2010).

[17] M. Sigrist, lecture notes: *Festkörperphysik - Theorie*, ETH Zürich, (2009).

[18] U.-J. Wiese, lecture notes: *Quantum Mechanics*, Universität Bern, (2010).

[19] K. S. Novoselov, Z. Jiang, Y. Zhang, S. V. Morozov, H. L. Stormer, U. Zeitler, J. C. Maan, G. S. Boebinger, P. Kim, A. K. Geim, arXiv:cond-mat/0702408v1 [cond-mat.mes-hall], (2007).

[20] Y. Zhang, T.-T. Tang, C. Girit, Z. Hao, M.C. Martin, A. Zettl, M.F. Crommie, Y.R. Shen, and F. Wang, Nature 459, 820 (2009).